inoculated with 1×10^6 cells of HT-29 or HCT-116 cell line in the flank region. The length (*a*) and width (*b*) of the tumor masses were measured twice a week, and the tumor volume (TV) was calculated as follows: $TV = (a \times b^2)/2$. All animal procedures were performed in compliance with the Guidelines for the Care and Use of Experimental Animals established by the Committee for Animal Experimentation of the National Cancer Center; these guidelines meet the ethical standards required by law and also comply with the guidelines for the use of experimental animals in Japan.

Drugs

The SN-38-incorporating polymeric micelles, NK012, and SN-38 were prepared by Nippon Kayaku (Tokyo, Japan).[12] CPT-11 was purchased from Yakult Honsha (Tokyo, Japan). 5FU was purchased from Kyowa Hakko (Tokyo, Japan).

Cell growth inhibition assay

HT-29 cells were seeded in 96-well plates at a density of 2,000 cells/well in a final volume of 90 μL. Twenty-four hours after seeding, a graded concentration of NK012 or SN-38 was added concurrently with 5FU to the culture medium of the HT-29 cells in a final volume of 100 μL for drug interaction studies. The culture was maintained in the CO_2 incubator for an additional 72 hr. Then, cell growth inhibition was measured by the tetrazolium salt-based proliferation assay (WST assay; Wako Chemicals, Osaka, Japan). WST-1 labeling solution (10 μL) was added to each well and the plates were incubated at 37°C for 3 hr. The absorbance of the formazan product formed was detected at 450 nm in a 96-well spectrophotometric plate reader. Cell viability was measured and compared to that of the control cells. Each experiment was carried out in triplicate and was repeated at least 3 times. Data were averaged and normalized against the nontreated controls to generate dose-response curves.

Drug interaction analysis

The nature of interaction between NK012 or SN-38 and 5FU against HT-29 cells was evaluated by median-effect plot analyses and the combination index (CI) method of Chou and Talalay.[13] Data analysis was performed using the Calcusyn software (Biosoft, NY, USA). NK012 or SN-38 was combined with 5FU at a fixed ratio that spanned the individual IC_{50} values of each drug. The IC_{50} values were determined on the basis of the dose-response curves using the WST assay. For any given drug combination, the CI is known to represent the degree of synergy, additivity or antagonism. It is expressed in terms of fraction-affected (*Fa*) values, which represents the percentage of cells killed or inhibited by the drug. Isobologram equations and *Fa*/CI plots were constructed by computer analysis of the data generated from the median effect analysis. Each experiment was performed in triplicate with 6 gradations and was repeated at least 3 times. The resultant dose-response curves were averaged, to create a single composite dose-response curve for each combination.

In vivo analysis of the effects of NK012 combined with 5FU as compared to those of CPT-11 combined with 5FU

When the mean tumor volumes reached ~93 mm^3, the mice were randomly divided into test groups consisting of 5 mice per group (Day 0). The drugs were administered i.v. *via* the tail vein of the mice. In the groups administered NK012 or 5FU as single agents, the drug was administered on Days 0, 7 and 14. In the combined treatment groups, NK012 or CPT-11 was administered 24 hr before 5FU on Days 0, 7 and 14, according to the previously reported combination schedule for CPT-11 and 5FU.[14] Complete response (CR) was defined as tumor not detectable by palpation at 90 days after the start of treatment, at which time-point the mice were sacrificed. Tumor volume and body weight were measured twice a week. As a general rule, animals in which the tumor volume exceeded 2,000 mm^3 were also sacrificed.

Experiment 1. Evaluation of the effects of NK012 combined with 5FU and determination of the maximum tolerated dose (MTD) of NK012/5FU. By comparing the data between NK012 administered as a single agent and NK012/5FU, we evaluated the effects of the combined regimen against the s.c HT-29 tumors. A preliminary experiment showed that combined administration of NK012 15 mg/kg + 5FU 50 mg/kg every 6 days caused drug-related lethality (data not shown). To determine the MTD, therefore, we set the dosing schedule of the combined regimen at 5 or 10 mg/kg of NK012 + 50 mg/kg of 5FU three times a week.

Experiment 2. Comparison of the antitumor effect of NK012/5FU and CPT-11/5FU. Based on a comparison of the data between NK012/5FU and CPT-11/5FU against the s.c. HT-29 and HCT-116 tumors, we investigated the feasibility of the clinical application of NK012/5FU for the treatment of CRC. CPT-11/5FU was administered three times a week at the respective MTDs of the 2 drugs as previously reported, that is, CPT11 at 50 mg/kg and 5FU at 50 mg/kg, respectively.[14] NK012/5FU was administered once three times a week at the respective MTDs of the 2 drugs determined from Experiment 1.

Cell cycle analysis

Samples from the HT-29 tumors that had grown to 80–100 mm^3 were removed from the mice at 6, 24, 48, 72 and 96 hr after the administration of NK012 alone at 10 mg/kg or CPT-11 alone at 50 mg/kg. The samples were excised, minced in PBS and fixed in 70% ethanol at −20°C for 48 hr. They were then digested with 0.04% pepsin (Sigma chemical Co., St Lous, MO) in 0.1 N HCL for 60 min at 37°C in a shaking bath to prepare single-nuclei suspensions. The nuclei were then centrifuged, washed twice with PBS and stained with 40 μg/mL of propidium iodide (Molecular Probes, OR) in the presence of 100 μg/mL RNase in 1 mL PBS for 30 min at 37°C. The stained nuclei were analyzed with B-D FACSCalibur (BD Biosciences, San Jose, CA), and the cell cycle distribution was analyzed using the Modfit program (Verity Software House Topsham, ME).

Statistical analyses

Data were expressed as mean ± SD. Data were analysed with Student's *t* test when the groups showed equal variances (*F* test), or Welch's test when they showed unequal variances (*F* test). $p < 0.05$ was regarded as statistically significant. All statistical tests were 2-sided.

Results

Antiproliferative effects of NK012 or SN-38 administered in combination with 5FU

Figure 1*a* shows the dose-response curves for NK012 alone, 5FU alone and a combination of the two. The IC_{50} levels of NK012 and 5FU against the HT-29 cells were 39 nM and 1 μM, respectively, and the IC_{50} level of SN-38 was 14 nM (data not shown). Based on these data, the molar ratio of NK012 or SN-38:5FU of 1:1,000 was used for the drug combination studies.

Figures 1*b* and 1*c* show the median-effect and the combination index plots. Combination indices (CIs) of <1.0 are indicative of synergistic interactions between 2 agents; additive interactions are indicated by CIs of 1.0, and antagonism by CIs of >1.0. Figure 1*c* shows the combination index for NK012 and 5FU, when 2 drugs are supposed to be mutually exclusive. Marked synergism was observed between Fa 0.2 and 0.6. Theoretically, the CI method is the most reliable around an Fa of 0.5, suggesting synergistic effects of the combination of NK012 and 5FU. This synergistic effect was more evident than that of SN-38/5FU (Fig. 1*d*).

In vivo *effect of combined NK012 and 5FU*

Experiment 1. Dose optimization and effect of combined NK012 and 5FU against HT-29 tumors. Comparison of the relative tumor volumes on Day 40 revealed significant differences between

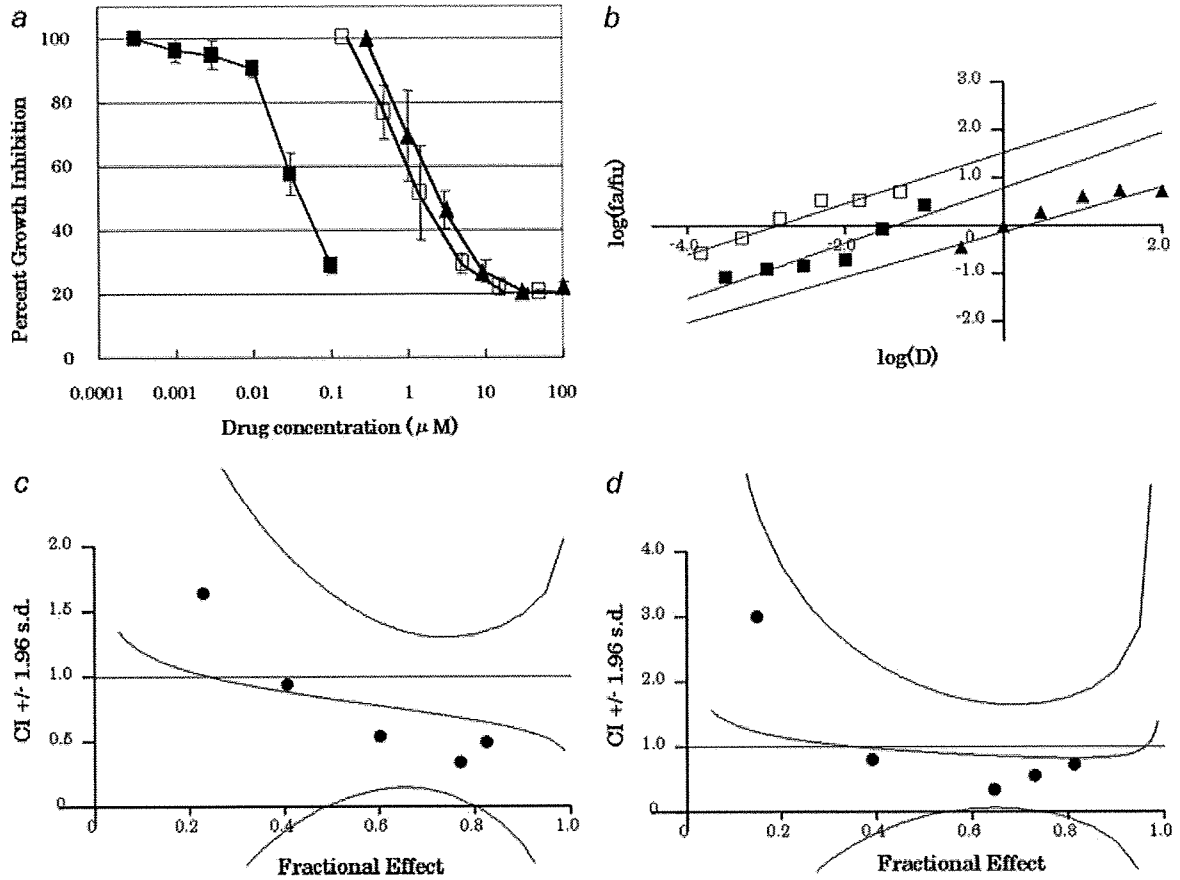

FIGURE 1 – Interaction of NK012 and 5FU *in vitro*. (*a*) Dose-response curves for NK012 alone (■), 5FU alone (▲) and their combination (□) against HT-29 cells. HT-29 cells were seeded at 2,000 cells/well. Twenty-four hours after seeding, a graded concentration of NK012 or 5FU was added to the culture medium of the HT-29 cells. Cell growth inhibition was measured by WST assay after 72 hr of treatment. Cell viability was measured and compared with that of the control cells. Each experiment was carried out independently and repeated at least 3 times. Points, mean of tripricates; bars, SD. (*b*) Median effect plot for the interaction of NK012 and 5FU. (*c*, *d*) Combination index for the interaction as a function of the level of effect (fraction effect = 0.5 is the IC_{50}). The straight line across the CI value of 1.0 indicates additive effect and CIs above and below indicate antagonism and synergism, respectively. The molar ratio of NK012/5FU (*c*) or SN-38/5FU (*d*) at 1:1,000 was tested by CI analysis. Black circles represent the CIs of the actual data points, solid lines represent the computer-derived CIs at effect levels ranging from 10 to 100% inhibition of cell growth, and the dotted lines represent the 95% confidence intervals.

those in the mice administered NK012 alone and those administered NK012/5FU at 5 mg/kg of NK012 ($p = 0.018$) (Fig. 2*a*). Although there was no statistically significant difference in the relative tumor volume measured on Day 54 between the mice administered NK012 alone and NK012/5FU at 10 mg/kg of NK012 ($p = 0.3050$), a trend of superior antitumor effect was demonstrated in the group treated with NK012/5FU at 10 mg/kg of NK012 (Fig. 2*a*). The CR rates were 20, 40 and 60% for 5 mg/kg NK012 + 50 mg/kg 5FU, 10 mg/kg NK012 alone and 10 mg/kg NK012 + 50 mg/kg 5FU, respectively. The schedule of 10 mg/kg NK012 + 50 mg/kg 5FU resulted in no remarkable toxicity in terms of body weight changes, and these doses were determined as representing the MTDs (Fig. 2*b*).

Experiment 2. Comparison of the antitumor effect of combined NK012/5FU and CPT-11/5FU against HT-29 and HCT-116 tumors. The therapeutic effect of NK012/5FU on Day 60 was significantly superior to that of CPT-11/5FU against the HT-29 tumors ($p = 0.0004$) (Fig. 3*a*). A more potent antitumor effect, namely, a 100% CR rate, was obtained in the NK012/5FU group as compared to the 0% CR rate in the CPT-11/5FU group. Although no statistically significant difference in the relative tumor volume on Day 61 was demonstrated between the NK012/5FU and CPT-11/5FU in the case of the HCT-116 tumors ($p = 0.2230$), a trend of superior antitumor effect against these tumors was observed in the NK012/5FU treatment group (Fig. 3*b*). The CR rates for the case of the HCT-116 tumors were 0% in both NK012/5FU and CPT-11/5FU groups.

Specificity of cell cycle perturbation

We studied the differences in the effects between NK012 10 mg/kg and CPT-11 50 mg/kg on the cell cycle (Fig. 4*a*). The data indicated that both NK012 and CPT-11 tended to cause accumulation of cells in the S phase, although the effect of NK012 was stronger and maintained for a more prolonged period than that of CPT-11; the maximal percentage of S-phase cells in the total cell population in the tumors was 34% at 24 hr after the administration of CPT-11, whereas it was 39% at 48 hr after the administration of NK012 (Figs. 4*b*, and 4*c*).

Discussion

Our primary endpoint was to clarify the advantages of NK012 over CPT-11 administered in combination with 5FU. We demonstrated that combined NK012 and 5FU chemotherapy exerts more

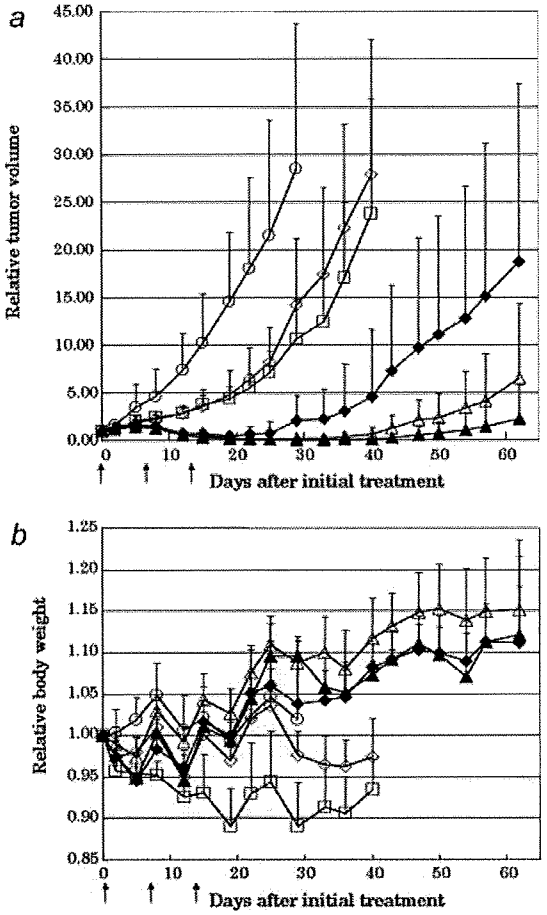

FIGURE 2 – Effect of NK012 alone or NK012 in combination with 5FU against HT-29 tumor-bearing mice. Points, mean; bars, SD. (*a*) Antitumor effect of each regimen on Days 0, 7 and 14. (○) control, (□) 5FU 50 mg/kg alone, (◇) NK012 5 mg/kg alone, (◆) NK012 5 mg/kg 24 hr before 5FU 50 mg/kg, (△) NK012 10 mg/kg alone, (▲) NK012 10 mg/kg 24 hr before 5FU 50 mg/kg. (*b*) Changes in the relative body weight. Data were derived from the same mice as those used in the present study.

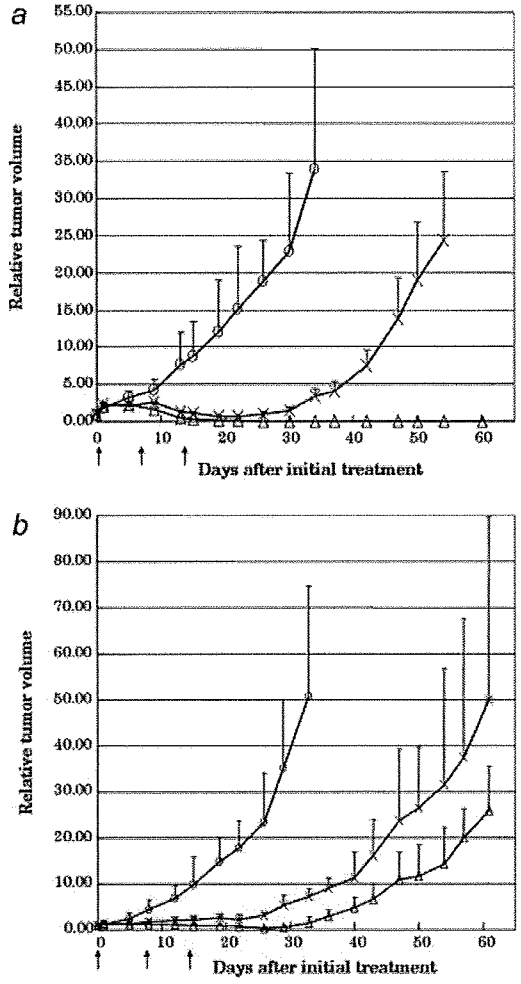

FIGURE 3 – Effect of NK012/5FU as compared with that of CPT11/5FU against HT-29 (*a*) or HCT-116 (*b*) tumor-bearing mice. Antitumor effect of each schedule on Days 0, 7 and 14. (○) control, (×) CPT-11 50 mg/kg 24 hr before 5FU 50 mg/kg, (△) NK012 10 mg/kg 24 hr before 5FU 50 mg/kg. Points, mean; bars, SD.

synergistic activity *in vitro* and significantly greater antitumor activity against human CRC xenografts as compared to CPT-11/5FU. The combination of NK012 and 5FU is considered to hold promise of clinical benefit for patients with CRC.

CPT-11, a topoisomerase-I inhibitor, and 5FU, a thymidilate synthase inhibitor, have been demonstrated to be effective agents for the treatment of CRC. A combination of these 2 drugs has also been demonstrated to be clearly more effective than either CPT-11 or 5FU/LV administered alone *in vivo* and in clinical settings.[1,2,14] Administration of 5FU by infusion with CPT-11 was shown to be associated with reduced toxicity and an apparent improvement in survival as compared to that of administration of the drug by bolus injection with CPT-11.[1,2] This synergistic enhancement may result from the mechanism of action of the 2 drugs; CPT-11 has been reported to cause accumulation of cells in the S phase, and 5FU infusion is known to cause DNA damage specifically in cells of the S phase.[14] On the basis of this background, our results suggesting the more pronounced and more prolonged accumulation of the tumor cells in the S phase caused by NK012 as compared with that by CPT-11 may explain the more effective synergy of the former administered with 5FU infusion. This may be attributable to accumulation of NK012 due to the enhanced permeability and retention (EPR) effect.[9] It is also speculated that NK012 allows sustained release of free SN-38, which may move more freely in the tumor interstitium.[15] Otherwise NK012 itself could internalize into cells to localize in several cytoplasmic organelles as reported by Savic *et al.*[16] These characteristics of NK012 may be responsible for its more potent antitumor activity observed in this study, because CPT-11 has been reported to show time-dependent growth-inhibitory activity against the tumor cells.[17]

The major dose-limiting toxicities of CPT-11 are diarrhea and neutropenia. SN-38, the active metabolite of CPT-11, may cause CPT-11-related diarrhea as a result of mitotic -inhibitory activity.[18] Because it undergoes significant biliary excretion, SN-38 may have a potentially long residence time in the gastrointestinal tract that may be associated with prolonged diarrhea.[19,20] In our previous report, we evaluated the tissue distribution of SN-38 after administration of an equimolar amount of NK012 (20 mg/kg) and CPT-11 (30 mg/kg), and found no difference in the level of SN-38 accumulation in the small intestine.[12] A significant antitumor effect of NK012 with a lower incidence of diarrhea was also dem-

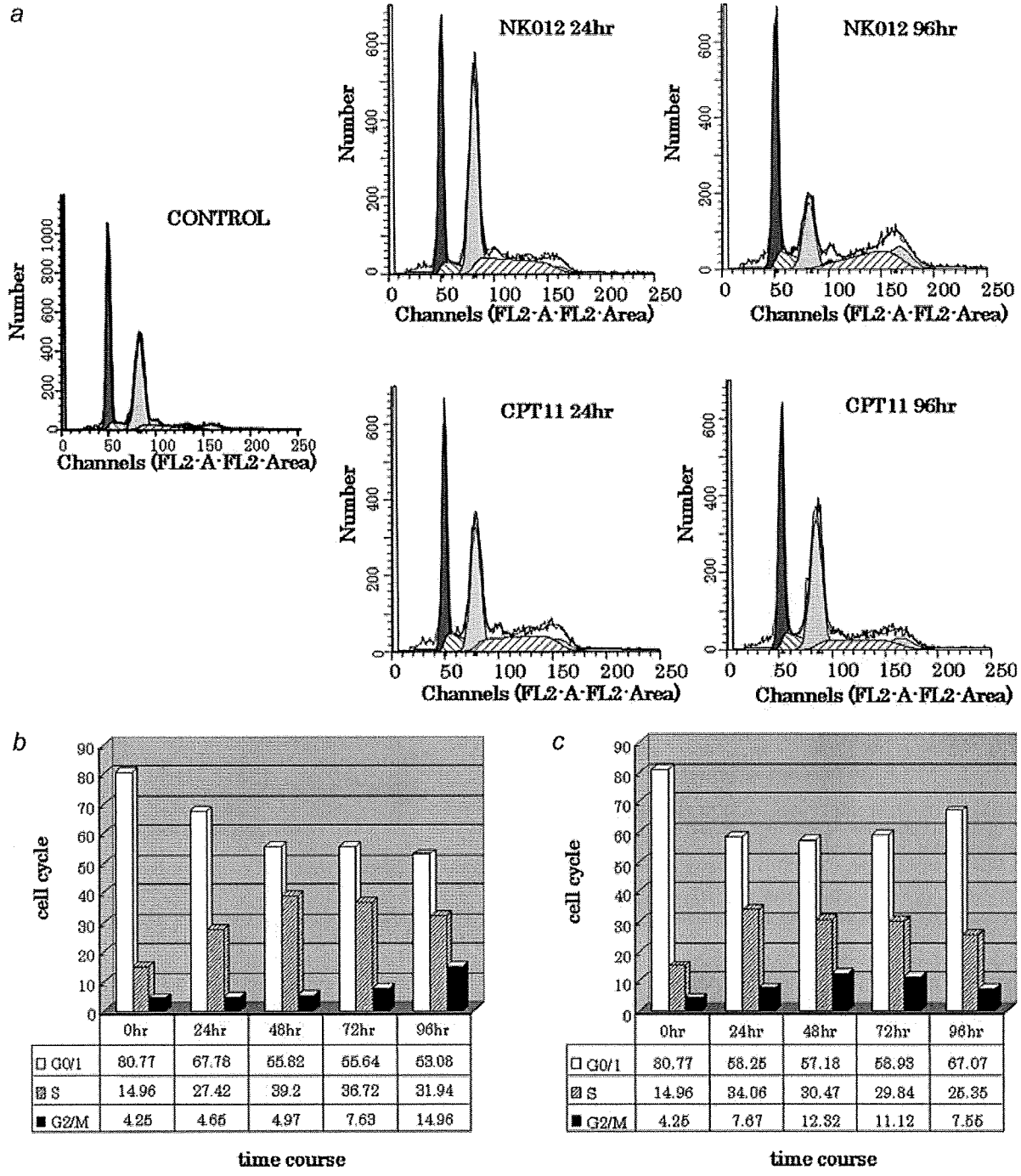

	0hr	24hr	48hr	72hr	96hr
G0/1	80.77	67.78	55.82	55.64	53.08
S	14.96	27.42	39.2	36.72	31.94
G2/M	4.25	4.65	4.97	7.63	14.96

	0hr	24hr	48hr	72hr	96hr
G0/1	80.77	58.25	57.18	58.93	67.07
S	14.96	34.06	30.47	29.84	25.35
G2/M	4.25	7.67	12.32	11.12	7.55

FIGURE 4 – Cell cycle analysis of HT-29 tumor cells collected 24, 48, 72 and 96 hr after administration of NK012 at 10 mg/kg alone or CPT-11 at 50 mg/kg alone using the Modfit program (Verity Software House Topsham, ME). (*a*) Cell cycle analysis of HT-29 tumor cells 24 and 96 hr after administration of NK012 at 10 mg/kg or CPT-11 at 50 mg/kg, respectively. (*b*) Cell cycle distribution of tumor cells 0, 24, 48, 72 and 96 hr after treatment with NK012 at 10 mg/kg. (*c*) Cell cycle distribution of tumor cells 0, 24, 48, 72 and 96 hr after treatment with CPT-11 at 50 mg/kg.

onstrated as compared to that observed with CPT-11 in a rat mammary tumor model.[21] Combined administration of CPT-11 with 5FU/LV infusion appears to be associated with acceptable toxicity in patients with CRC. In addition, no significant difference in the frequency of Grade 3/4 diarrhea was noted between patients treated with FOLFIRI (CPT-11 regimen with bolus and infusional 5FU/LV) and those treated with FOLFOX6 (oxaliplatin regimen with bolus and infusional 5FU/LV).[22,23] Our *in vivo* data actually revealed no severe body weight loss in the NK012/5FU group. Consequently, we expect that the NK012/5FU regimen, especially

with infusional 5FU, may be an attractive arm for a Phase III trial in CRC, with CPT-11/5FU as the control arm. We have already initiated a Phase I trial of NK012 in patients with advanced solid tumors based on the data suggesting higher efficacy and lower toxicity of this preparation than CPT-11 *in vivo*.[12]

In conclusion, we demonstrated that combined NK012 and 5FU chemotherapy exerts significantly greater antitumor activity against human CRC xenografts as compared to CPT-11/5FU, indicating the necessity of clinical evaluation of this combined regimen.

References

1. Saltz LB, Douillard JY, Pirotta N, Alakl M, Gruia G, Awad L, Elfring GL, Locker PK, Miller LL. Irinotecan plus fluorouracil/leucovorin for metastatic colorectal cancer: a new survival standard. Oncologist 2001;6:81–91.
2. Douillard JY, Cunningham D, Roth AD, Navarro M, James RD, Karasek P, Jandik P, Iveson T, Carmichael J, Alakl M, Gruia G, Awad L, et al. Irinotecan combined with fluorouracil compared with fluorouracil alone as first-line treatment for metastatic colorectal cancer: a multicentre randomised trial. Lancet 2000;355:1041–7.
3. Takimoto CH, Arbuck SG. Topoisomerase I targeting agents: the camptothecins. In: Chabner BA, Lango DL, eds. Cancer chemotherapy and biotherapy: principal and practice, 3rd ed. Philadelphia, PA: Lippincott Williams and Wilkins, 2001. 579–646.
4. Slatter JG, Schaaf LJ, Sams JP, Feenstra KL, Johnson MG, Bombardt PA, Cathcart KS, Verburg MT, Pearson LK, Compton LD, Miller LL, Baker DS, et al. Pharmacokinetics, metabolism, and excretion of irinotecan (CPT-11) following I.V. infusion of [(14)C]CPT-11 in cancer patients. Drug Metab Dispos 2000;28:423–33.
5. Rothenberg ML, Kuhn JG, Burris HA, III, Nelson J, Eckardt JR, Tristan-Morales M, Hilsenbeck SG, Weiss GR, Smith LS, Rodriguez GI, Rock MK, Von Hoff DD. Phase I and pharmacokinetic trial of weekly CPT-11. J Clin Oncol 1993;11:2194–204.
6. Guichard S, Terret C, Hennebelle I, Lochon I, Chevreau P, Fretigny E, Selves J, Chatelut E, Bugat R, Canal P. CPT-11 converting carboxylesterase and topoisomerase activities in tumour and normal colon and liver tissues. Br J Cancer 1999;80:364–70.
7. Gradishar WJ, Tjulandin S, Davidson N, Shaw H, Desai N, Bhar P, Hawkins M, O'Shaughnessy J. Phase III trial of nanoparticle albumin-bound paclitaxel compared with polyethylated castor oil-based paclitaxel in women with breast cancer. J Clin Oncol 2005;23:7794–803.
8. Muggia FM. Liposomal encapsulated anthracyclines: new therapeutic horizons. Curr Oncol Rep 2001;3:156–62.
9. Matsumura Y, Maeda H. A new concept for macromolecular therapeutics in cancer chemotherapy: mechanism of tumoritropic accumulation of proteins and the antitumor agent smancs. Cancer Res 1986;46:6387–92.
10. Zhang JA, Xuan T, Parmar M, Ma L, Ugwu S, Ali S, Ahmad I. Development and characterization of a novel liposome-based formulation of SN-38. Int J Pharm 2004;270:93–107.
11. Kraut EH, Fishman MN, LoRusso PM, Gorden MS, Rubin EH, Haas A, Fetterly GJ, Cullinan P, Dul JL, Steinberg JL. Final result of a phase I study of liposome encapsulated SN-38 (LE-SN38): safety, pharmacogenomics, pharmacokinetics, and tumor response [abstract 2017]. Proc Am Soc Clin Oncol 2005;23:139S.
12. Koizumi F, Kitagawa M, Negishi T, Onda T, Matsumoto S, Hamaguchi T, Matsumura Y. Novel SN-38-incorporating polymeric micelles, NK012, eradicate vascular endothelial growth factor-secreting bulky tumors. Cancer Res 2006;66:10048–56.
13. Chou TC, Talalay P. Quantitative analysis of dose-effect relationships: the combined effects of multiple drugs or enzyme inhibitors. Adv Enzyme Regul 1984;22:27–55.
14. Azrak RG, Cao S, Slocum HK, Toth K, Durrani FA, Yin MB, Pendyala L, Zhang W, McLeod HL, Rustum YM. Therapeutic synergy between irinotecan and 5-fluorouracil against human tumor xenografts. Clin Cancer Res 2004;10:1121–9.
15. Jain RK. Barriers to drug delivery in solid tumors. Sci Am 1994; 271:58–65.
16. Savic R, Luo L, Eisenberg A, Maysinger D. Micellar nanocontainers distribute to defined cytoplasmic organelles. Science 2003;300:615–18.
17. Kawato Y, Aonuma M, Hirota Y, Kuga H, Sato K. Intracellular roles of SN-38, a metabolite of the camptothecin derivative CPT-11, in the antitumor effect of CPT-11. Cancer Res 1991;51:4187–91.
18. Slater R, Radstone D, Matthews L, McDaid J, Majeed A. Hepatic resection for colorectal liver metastasis after downstaging with irinotecan improves survival. Proc Am Soc Clin Oncol 2003;22(abstract 1287).
19. Araki E, Ishikawa M, Iigo M, Koide T, Itabashi M, Hoshi A. Relationship between development of diarrhea and the concentration of SN-38, an active metabolite of CPT-11, in the intestine and the blood plasma of athymic mice following intraperitoneal administration of CPT-11. Jpn J Cancer Res 1993;84:697–702.
20. Atsumi R, Suzuki W, Hakusui H. Identification of the metabolites of irinotecan, a new derivative of camptothecin, in rat bile and its biliary excretion. Xenobiotica 1991;21:1159–69.
21. Onda T, Nakamura I, Seno C, Matsumoto S, Kitagawa M, Okamoto K, Nishikawa K, Suzuki M. Superior antitumor activity of NK012, 7-ethyl-10-hydroxycamptoyhecin-incorporating micellar nanoparticle, to irrinotecan. Proc Am Assoc Cancer Res 2006;47:720s(abstract 3062).
22. Tournigand C, Andre T, Achille E, Lledo G, Flesh M, Mery-Mignard D, Quinaux E, Couteau C, Buyse M, Ganem G, Landi B, Colin P, et al. FOLFIRI followed by FOLFOX6 or the reverse sequence in advanced colorectal cancer: a randomized GERCOR study. J Clin Oncol 2004;22:229–37.
23. Colucci G, Gebbia V, Paoletti G, Giuliani F, Caruso M, Gebbia N, Carteni G, Agostara B, Pezzella G, Manzione L, Borsellino N, Misino A, et al. Phase III randomized trial of FOLFIRI versus FOLFOX4 in the treatment of advanced colorectal cancer: a multicenter study of the Gruppo Oncologico Dell'Italia Meridionale. J Clin Oncol 2005; 23:4866–75.

British Journal of Cancer (2008) 99, 2020–2028

www.bjcancer.com

KRAS or *BRAF* mutation status is a useful predictor of sensitivity to MEK inhibition in ovarian cancer

N Nakayama[1], K Nakayama*[,1], S Yeasmin[1], M Ishibashi[1], A Katagiri[1], K Iida[1], M Fukumoto[2] and K Miyazaki[1]

[1]Departments of Obstetrics and Gynecology, Shimane University School of Medicine, Izumo, Japan; [2]Departments of Pathology, Institute of Development, Aging and Cancer, Tohoku University, Sendai, Japan

This study examined the status of *KRAS* and *BRAF* mutations, in relation to extracellular signal-regulated protein kinase (ERK) activation in 58 ovarian carcinomas to clarify the clinicopathological and prognostic significance of *KRAS/BRAF* mutations. Somatic mutations of either *KRAS* or *BRAF* were identified in 12 (20.6%) out of 58 ovarian carcinomas. The frequency of *KRAS/BRAF* mutations in conventional serous high-grade carcinomas (4.0%: 1/25) was significantly lower than that in the other histological type (32.3%: 10/31). Phosphorylated ERK1/2 (p-ERK1/2) expression was identified in 18 (38.2%) out of 45 ovarian carcinomas. *KRAS/BRAF* mutation was significantly correlated with International Federation of Gynecology and Obstetrics (FIGO) stage I, II ($P<0.001$), and p-ERK1/2 ($P<0.001$). No significant correlations between *KRAS/BRAF* mutations or p-ERK1/2 expression and overall survival were found in patients with ovarian carcinoma treated with platinum and taxane chemotherapy ($P=0.2460$, $P=0.9339$, respectively). Next, to clarify the roles of ERK1/2 activation in ovarian cancers harbouring *KRAS* or *BRAF* mutations, we inactivated ERK1/2 in ovarian cancer cells using CI-1040. CI-1040 is a compound that selectively inhibits MAP kinase kinase (MEK), an upstream regulator of ERK1/2, and thus prevents ERK1/2 activation. Profound growth inhibition and apoptosis were observed in CI-1040-treated cancer cells with mutations in either *KRAS* or *BRAF* in comparison with the ovarian cancer cells containing wild-type sequences. This was evident in both *in vitro* and *in vivo* studies. The findings in this study indicate that an activated ERK1/2 pathway is critical to tumour growth and survival of ovarian cancers with *KRAS* or *BRAF* mutations. Furthermore, they suggest that the CI-1040-induced phenotypes depend on the mutational status of *KRAS* and *BRAF* in ovarian cancers. Therefore, ovarian cancer patients with *KRAS* or *BRAF* mutations may benefit from CI-1040 treatment.

British Journal of Cancer (2008) **99,** 2020–2028. doi:10.1038/sj.bjc.6604783 www.bjcancer.com
Published online 18 November 2008

Keywords: ovarian carcinoma; *KRAS*; *BRAF*; mutation; ERK1/2; CI-1040

Translational Therapeutics

Ovarian carcinoma is the most lethal malignant disease in American women (Wingo *et al*, 1995) and the most lethal gynaecological cancer in Japan. Its frequency has increased dramatically in the last decade. In more than 70% of patients with ovarian carcinoma, there is evidence of tumour dissemination beyond the ovaries at diagnosis. In these cases, combined treatment with surgery and chemotherapy is necessary. First-line chemotherapy with platinum drugs and taxanes yields a response rate of over 80%, but almost all patients relapse. Although there are well-established surgical and chemotherapeutic treatments for ovarian cancer, there is a significant opportunity to develop drugs targeting specific molecular pathways. Drugs of this type would be particularly useful for recurrent disease that has acquired chemoresistance. Thus, there is a need for an improved understanding of the molecular pathways of ovarian carcinogenesis. Several genetic alterations are associated with ovarian carcinogenesis. The most frequent genetic abnormalities in ovarian carcinoma are mutations in *KRAS*, *BRAF*, and *p53* (Singer *et al*, 2003; Nakayama *et al*, 2006).

*Correspondence: Dr K Nakayama,Shimane University School of Medicine, Enyacho 89-1, Izumo, Shimane, Japan 6938501;
E-mail: kn88@med.shimane-u.ac.jp
Revised 10 October 2008; accepted 21 October 2008; published online 18 November 2008

Mutations of either *BRAF* or *KRAS* lead to constitutive activation (phosphorylation) of their downstream target, mitogen-activated protein kinase (MAPK), also known as extracellular signal-regulated protein kinase (ERK) (Olson and Hallahan, 2004; Wan *et al*, 2004). Mutations in *BRAF* or *KRAS* are correlated with overexpression of activated ERK1/2 in ovarian serous tumours (Hsu *et al*, 2004). Activation of ERK1/2 in turn activates downstream cellular targets (Peyssonnaux and Eychene, 2001; Allen *et al*, 2003) including a variety of cellular and nuclear proteins. Although the functions of the RAS–RAF–MEK–ERK pathway and its downstream effectors have been recently explored, only the serous type of ovarian cancer has been studied (Hsu *et al*, 2004; Pohl *et al*, 2005). In addition, the biological role of this pathway in the development of ovarian cancers of other histological types is unknown.

Activating *KRAS* and *BRAF* mutations typically show mutant exclusivity in tumours (Brose *et al*, 2002; Davies *et al*, 2002; Gorden *et al*, 2003; Singer *et al*, 2003).

A large proportion of microsatellite-stable colorectal tumour metastases has been shown to accumulate *BRAF/KRAS* mutations (Oliveira *et al*, 2007). This suggests an epistatic relationship in which either mutation is sufficient to deregulate a common effector pathway, such as the MAP kinase kinase (MEK)–ERK kinase cascade. If this is the case, tumours arising as a result of a mutation in either *KRAS* or *BRAF* should harbour similar

downstream dependencies. These might represent useful therapeutic targets in ovarian cancer. To test this hypothesis, we examined the consequences of MEK–ERK pathway inhibition using a highly potent and selective inhibitor of MEK1/2, CI-1040 (formerly known as PD184352) (Schaeffer and Weber, 1999; Sebolt-Leopold *et al*, 1999, 2003; Sebolt-Leopold, 2004). The inhibitor was tested in a collection of ovarian cancer cell lines that showed differing mechanisms of MAP kinase pathway deregulation.

MATERIALS AND METHODS

Tissue samples

Formalin-fixed, paraffin-embedded tissue samples of 58 ovarian cancers, including 27 serous carcinomas, 20 mucinous carcinomas, and 11 endometrioid carcinomas were used in this study. These samples were obtained from the Department of Obstetrics and Gynecology at the Shimane University Hospital. Diagnosis was based on conventional morphological examination of sections stained with haematoxylin and eosin (H&E) staining, and tumours were classified according to the WHO (World Health Organization) classification. Tumour staging was carried out according to the International Federation of Gynecology and Obstetrics (FIGO) classification. The clinicopathological characteristics of the patients included in this study are summarised in Table 1. All the patients were primarily treated with cytoreductive surgery and adjuvant platinum and taxane chemotherapy (CBDCA AUC5, Paclitaxel 175 mg m^{-2} or Docetaxel 70 mg m^{-2}). All the cases received 6–12 courses of this regimen. The acquisition of tumour tissues was approved by the Shimane University Institutional Review Board. The paraffin tissue blocks were organised into tissue microarrays, which were made by removing 3 mm diameter cores of tumour from each block. The areas for coring were selected by surgical pathologists (MF) on the basis of a review of the H&E slides.

Cell culture and cell lines

OVCAR3, SKOV3, A2780, MDAH2774 (serous carcinoma), and ES2 (clear cell carcinoma) human ovarian cancer cell lines were obtained from the American Tissue Culture Center (Rockville, MD, USA). The human ovarian carcinoma cell line KF28 (serous carcinoma) was a kind gift from Dr Yoshihiro Kikuchi (Ohki Memorial Kikuchi Cancer Clinic for Women, Saitama, Japan) (Yamamoto *et al*, 2000). The MPSC1 cell line was established from a low-grade serous carcinoma and was a kind gift from Dr le-Ming Shih (Johns Hopkins Medical Institutions, Baltimore, MD, USA). OVK#18 (serous carcinoma) human ovarian cancer cell line was obtained from Tohoku University (Sendai, Japan). OMC3 (mucinous carcinoma) and JHOC5 (clear cell carcinoma) human ovarian cancer cell lines were also obtained from Riken Bioresource Center (Ibaragi, Japan). In addition, human papillomavirus E6/E7-immortalised primary cultures of normal ovarian surface epithelium (OSE) were also included in this study. IOSE27, a normal OSE cell line, was obtained from the American Tissue Culture Center. OSE7 and OSE10 normal OSE cell lines were a kind gift from Dr Hidetaka Katabuchi (Kumamoto University, Kumamoto, Japan).

A set of primary cultures was established from ovarian cancers, including POC-1, POC-2, and POC-3. The acquisition of anonymous tissue specimens was approved by the Shimane University Institutional Review Board.

The diagnoses were confirmed by a surgical pathologist before the tumour samples were harvested for experiments. Primary tumour cultures were established from freshly isolated tumour samples by immunosorting or trypsinisation. For immunosorting, fresh tumour tissues were minced and incubated with collagenase

Table 1 Mutational status of *KRAS* and *BRAF* genes and p-ERK1/2 expression in ovarian cancer

Case no.	Histology	Grade	*KRAS*	*BRAF*	p-ERK1/2
1	Serous	1	WT	WT	N
2	Serous	1	WT	T1796A/V600E	P
3	Serous	2	WT	WT	N
4	Serous	3	WT	WT	N
5	Serous	3	WT	WT	N
6	Serous	2	WT	WT	P
7	Serous	2	WT	WT	N
8	Serous	2	WT	WT	P
9	Serous	3	WT	WT	N
10	Serous	3	WT	WT	P
11	Serous	3	WT	WT	P
12	Serous	3	WT	WT	N
13	Serous	3	WT	WT	N
14	Serous	3	G35T/G12V	WT	P
15	Serous	3	WT	WT	N
16	Serous	3	WT	WT	N
17	Serous	3	WT	WT	N
18	Serous	3	WT	WT	P
19	Serous	3	WT	WT	N
20	Serous	3	WT	WT	N
21	Serous	3	WT	WT	N
22	Serous	3	WT	WT	P
23	Serous	3	WT	WT	P
24	Serous	3	WT	WT	N
25	Serous	3	WT	WT	N
26	Serous	3	WT	WT	P
27	Serous	3	WT	WT	P
28	Mucinous	1	WT	T1796A/V600E	P
29	Mucinous	1	G35A/G12D	T1796A/V600E	P
30	Mucinous	1	WT	WT	N
31	Mucinous	1	WT	T1796A/V600E	P
32	Mucinous	1	G35T/G12V	WT	P
33	Mucinous	2	WT	WT	N
34	Mucinous	2	WT	WT	N
35	Mucinous	2	G35A/G12D	WT	P
36	Mucinous	2	WT	WT	N
37	Mucinous	2	WT	WT	N
38	Mucinous	2	WT	WT	N
39	Mucinous	2	WT	WT	N
40	Mucinous	2	WT	WT	P
41	Mucinous	3	WT	WT	P
42	Mucinous	3	WT	WT	N
43	Mucinous	3	WT	WT	N
44	Mucinous	3	WT	WT	N
45	Mucinous	3	WT	WT	N
46	Mucinous	3	WT	WT	P
47	Mucinous	3	WT	WT	N
48	Endometrioid	1	WT	T1796A/V600E	P
49	Endometrioid	1	WT	WT	N
50	Endometrioid	2	WT	WT	P
51	Endometrioid	2	WT	WT	N
52	Endometrioid	2	G35A/G12D	WT	P
53	Endometrioid	2	G35A/G12D	WT	P
54	Endometrioid	2	G35T/G12V	WT	P
55	Endometrioid	3	G35A/G12D	WT	P
56	Endometrioid	3	WT	WT	N
57	Endometrioid	3	WT	WT	P
58	Endometrioid	3	WT	WT	N

N = negative; P = positive; WT = wild type.

A (2 mg ml^{-1}) at 37 °C for 40 min. After filtration through sieve membranes (with 100 μm pores), tumour cells were immunosorted using an epithelial specific antigen (Ep-CAM) antibody bound to Dynal™ beads (Dynal, Oslo, Norway) following the vendor's instructions (Nakayama *et al*, 2006). Freshly isolated tumour cells were allowed to grow in culture and were used for experiments within two passages.

Mutational analysis of *KRAS* and *BRAF*

Genomic DNA was purified from all the cell lines and formalin-fixed, paraffin-embedded tissues using a Qiaquick polymerase chain reaction (PCR) purification kit (Qiagen, Valencia, CA, USA). PCR was then carried out followed by nucleotide sequencing using the iCycler (Bio-Rad, Hercules, CA, USA). Exon 1 of *KRAS* and exon 15 of *BRAF* were both sequenced, as these mutational hot spots together harbour nearly all published mutations (Davies *et al*, 2002; Singer *et al*, 2002, 2003; Sieben *et al*, 2004). The primers for PCR and sequencing were manufactured by GeneLink (Hawthorne, NY, USA), and their sequences were described in an earlier report (Nakayama *et al*, 2006). The sequences were analysed using the Lasergene programme, DNASTAR (Madison, WI, USA).

Immunohistochemistry

Expression of the active phosphorylated ERK1/2 (p-ERK1/2) was assessed by immunohistochemistry and western blot analysis. The antibody used in this study was a rabbit polyclonal antibody that reacted with phosphorylated but not unphosphorylated ERK1/2 (Cell Signaling Technology). Immunohistochemistry was carried out on tissue microarrays at a dilution of 1 : 1000 followed by detection with the En Vision + System using the peroxidase method (DAKO, Carpinteria, CA, USA). The percentage of positive cells was estimated by randomly counting ~500 tumour cells from three different high-power fields (× 40) within one specimen. A positive reaction was defined as a discrete localisation of the brown chromagen in the nucleus or cytoplasm. Cases in which more than 5% of the tumour cells showed detectable immunoreactivity were scored as positive.

Western blot analysis

Cell lysates were prepared by dissolving cell pellets in Laemmli sample buffer (BioRad, Hercules, CA, USA) supplemented with 5% β-mercaptoethanol (Sigma, St Louis, MO, USA). Western blot analysis was performed on ovarian cancer/OSE cell lines/cultures, including OVCAR3, SKOV3, A2780, MDAH2774, ES2, MPSC1, KF28, OVK#18, OMC3, JHOC5, PC1, PC2, PC3, IOSE29, OSE7, and OSE10. Similar amounts of total protein from each lysate were loaded and separated on 10% Tris-Glycine-SDS polyacrylamide gels (Novex, San Diego, CA, USA) and electroblotted to Millipore Immobilon-P polyvinylidene difluoride membranes. The membranes were probed with an active ERK1/2 antibody (pTEpY, 1 : 5000) (Cell Signaling Technology) followed by a peroxidase-conjugated anti-mouse or anti-rabbit immunoglobulin (1 : 20 000). The same membrane was probed with an antibody that reacted with total ERK1/2 (1 : 5000) (Cell Signaling Technology) for loading controls. Western blots were developed by chemiluminescence (Pierce, Rockford, IL, USA).

Cell-growth assays

For the cell-growth assay, cells were plated at the same density (3×10^3 cells per well) in 96-well plates. An methyl thiazoyl tetrazorium (MTT) cell-growth assay was performed (Nakayama *et al*, 2001) 96 h after treating the cells with CI-1040 (provided by Pfizer, Inc., New York, NY, USA) at 5 μM or with dimethyl sulphoxide (DMSO) (control). The data were expressed as a percentage of the DMSO control. The mean and standard deviation (s.d.) were obtained from three experiments. Apoptotic cells were detected with 4',6-diamidino-2-phenylindole (DAPI) staining. The data were expressed as the mean ± 1 s.d. from triplicates. To confirm the presence of apoptotic cells, DAPI-stained cells were also stained with Annexin V dye. Bromodeoxyuridine (BrdUrd) uptake and staining were measured using a cell proliferation kit (Amersham, Buckinghamshire, England, UK) and apoptotic cells were detected using an Annexin V staining kit (Bio Vision, Mountain View, CA, USA). The percentages of BrdUrd-positive and Annexin V-positive cells were determined by counting approximately 400 cells from each well in 96-well plates. The data were expressed as the mean ± 1 s.d. of triplicates.

Tumour xenograft in nude mice

To confirm the findings of a CI-1040 effect *in vitro*, we injected 3×10^6 MDAH2774 or SKOV3 cells into the intraperitoneal tissue of *nu/nu* mice (4 weeks of age). Four weeks BALB/c *nu/nu* mice were purchased from Charles River Japan Inc. (Kanagawa, Japan). CI-1040 was prepared in a vehicle of 10% Cremophore EL (Sigma, St Louis, MO, USA), 10% ethanol, and 80% water. When the model for the mouse study was first designed, the end point was set to be the day when the mice began to produce ascites, or acute gain of weight due to tumour growth, for reasons of ethical origin. Tumours that start causing ascites have a chance of developing other malignant characteristics, which can become harmful progressively. Four mice were used for each experimental group. During the study, the mice were killed when it was discovered that the abdomen of one of the mice had begun to distend because of ascites. One week after tumour-cell injection, either CI-1040 (CI-1040, 150 mg kg^{-1}, resuspended in 10% Cremophore EL (Sigma), 10% ethanol, and 80% water) or a vehicle only (10% Cremophore EL (Sigma), 10% ethanol, and 80% water) were injected intraperitoneally (i.p.) once daily for 3 weeks. The total dose of CI-1040 for each mouse was 63 mg. Four weeks after the cell injection (three weeks after CI-1040 injection), the abdomens of the control group mice had begun to distend. The time for termination of the experiment was dictated by the aforementioned ethical reasons (tumour ascites in controls), and this endpoint was observed at that time. We anaesthetised the mice before they were rendered moribund by the experiment. The total tumour weight at that time was around 500 mg. Necropsy was carried out on all mice to assess i.p. tumour growth, and the tumours were excised and weighed. Animal experiments were carried out in accordance with the regulations of the Institutional Ethical Commission (Shimane University) and of the United Kingdom Co-ordinating Committee on Cancer Research guidelines (Workman, 1998).

Statistical methods for clinical correlation

Overall survival was calculated from the date of diagnosis to the date of death or last follow-up. Patients with either *KRAS* or *BRAF* mutations had similar performance status distributions. The data were plotted as Kaplan–Meier curves, and the statistical significance was determined by the log-rank test. Data were censored when patients were lost to follow-up. The Student's *t*-test was used to examine the statistical significance in the difference of growth-assay data.

RESULTS

Identification of *KRAS* and *BRAF* mutations

The mutational status of *KRAS* and *BRAF* in all 45 ovarian carcinomas is summarised in Table 1. Somatic mutations of *KRAS* were identified in 8 (13.7%) out of 58 ovarian carcinomas. In

contrast, somatic mutations of *BRAF* were identified in 5 (8.6%) out of 58 ovarian carcinomas. Somatic mutations of either *KRAS* or *BRAF* were identified in 12 (20.6%) out of 58 ovarian carcinomas. Most *KRAS* mutations were located at codon 12 and all *BRAF* mutations at codon 600. Both of these codons are mutation hot spots. Interestingly, simultaneous mutations of *KRAS* and *BRAF* did not occur in the tested ovarian carcinomas with the exception of one mucinous case.

A panel of ovarian cancer cell lines and primary cultures was first analysed for tumour mutation status in the *KRAS* and *BRAF* genes. As shown in Figure 1, three ovarian cancer cell lines harboured either *KRAS* or *BRAF* mutations. The frequency of either *KRAS* or *BRAF* mutations in conventional serous high-grade carcinomas (4.0%: 1/25) was significantly lower than in the other histological type (32.2%: 10/31).

Relationship between *KRAS/BRAF* mutations and p-ERK1/2 expression or clinicopathological factors

The immunoreactivity of active p-ERK1/2 was detected in both the nucleus and the cytoplasm of the tumour cells (Figure 2). This is consistent with an earlier report (Mizumoto *et al*, 2007). Positive active p-ERK1/2 was identified in 27 (46.6%) out of 58 ovarian carcinomas. The patients were stratified into two groups depending on the mutational status of *KRAS/BRAF*. The relationships between *KRAS/BRAF* mutations and clinicopathological factors, including p-ERK1/2 expression are shown in Table 2. There was no significant correlation between *KRAS/BRAF* mutations and the patient's age. The results in Table 2 show that *KRAS/BRAF* mutation is correlated significantly with FIGO stage I, II ($P<0.001$), and p-ERK1/2 ($P<0.001$). In addition, there were significant correlations between *KRAS/BRA*F mutations and pathological grade ($P=0.004$), and histological subtype ($P=0.014$).

Effect of *KRAS/BRAF* mutations or p-ERK1/2 on the prognosis of ovarian carcinomas

Next, we examined the prognostic effect of *KRAS/BRAF* mutations and p-ERK1/2 expression. Out of the 58 samples that we examined, 45 were available for prognostic analysis. Kaplan–Meier estimates of overall survival are plotted in Figure 3. There was no significant relationship between *KRAS/BRAF* mutations or p-ERK1/2 expression and overall survival in patients with ovarian carcinoma ($P=0.2460$, $P=0.9339$, respectively). Univariate analysis showed that only FIGO stage III, IV affected the overall survival of patients with ovarian carcinoma significantly($P=0.014$).

Effects of ERK1/2 inactivation on ovarian carcinoma *in vitro*

A panel of ovarian cancer cell lines and primary cultures of ovarian cancer were first analysed for *KRAS* and *BRAF* gene mutation status. Mutational status was correlated with growth inhibition and apoptosis induction by the MEK inhibitor CI-1040 that prevented activation of the downstream target, ERK1/2. Western blot analysis showed a dose-dependent effect on the expression of active ERK1/2 in ES2 cells, and active ERK1/2 was not detectable 6 h after treating the cells with CI-1040 at a concentration of 5 μM (Figure 4). As shown in Figure 5, four of the tumours harbouring either *KRAS* or *BRAF* mutations showed a marked reduction (<50% of DMSO control) in the cell number in the CI-1040-treated group as compared with the other 14 tumours containing wild-type *KRAS* and *BRAF* ($P<0.001$). CI-1040 had no significant effect on the growth of normal cells, including the OSE cells. It is likely that *KRAS/BRAF* mutation is not the only determinant for activating ERK1/2. Therefore, we analysed p-ERK1/2 expression in each of the cell lines listed in Figure 5. Only four of these cell lines, MDAH2774, ES2, MPSC1, and POC1, strongly expressed p-ERK1/2. SKOV3 and A2780 showed weak expression of ERK1/2.These results suggest that activation of ERK1/2 may depend on *KRAS/BRAF* mutation in ovarian cancer cells.

To assess the mechanisms underlying growth inhibition by CI-1040, we measured the percentages of BrdUrd-labelled cells and Annexin V-labelled cells to estimate proliferation and apoptosis, respectively. We found that CI-1040 significantly reduced cellular proliferation and induced apoptosis in cell lines with either *KRAS* or *BRAF* mutations in comparison with cell lines with wild-type sequences (Figure 6, Supplementary Figure 1).

Effects of CI-1040 ERK1/2 inactivation on ovarian carcinomas *in vivo*

On the basis of the above findings, we investigated whether CI-1040 had a growth-inhibitory effect on tumour formation and development *in vivo*. Tumour xenografts from both MDAH2774 (*KRAS* mutant) and SKOV3 (wild type of *KRAS* and *BRAF*) cell

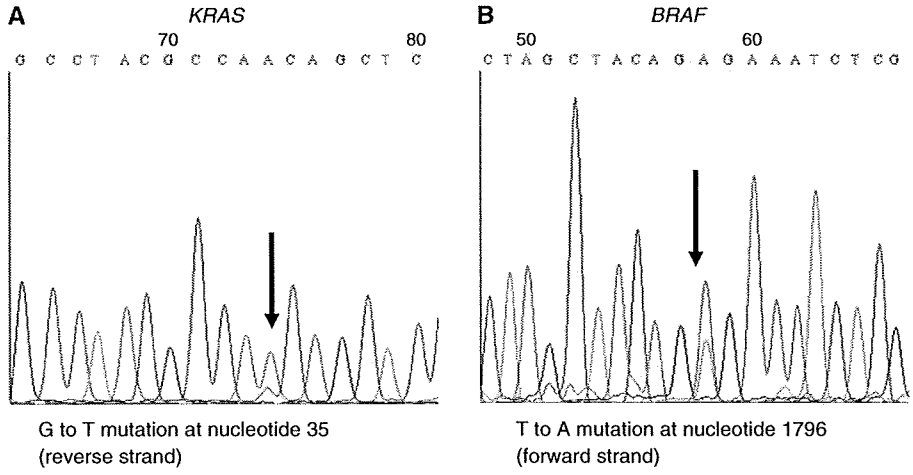

Figure 1 Chromatograms of *KRAS* and *BRAF* mutational status in three representative ovarian cancer cells. (**A**) Left panel (MDAH2774) showing a point mutation in the *KRAS* gene. (**B**) Right panel (ES2) showing a point mutation in the *BRAF* gene. Arrows represent spike which indicates mutation.

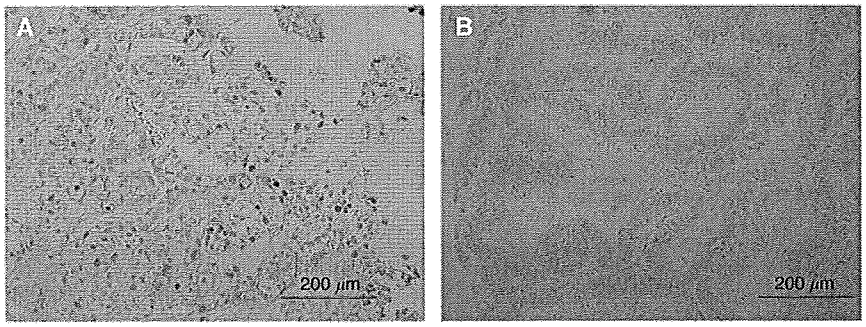

Figure 2 Immunohistochemical staining of phosphorylated extracellular-regulated kinase (p-ERK1/2). (**A**) Intense immunoreactivity is present in both the nucleus and the cytoplasm in this ovarian carcinoma. (**B**) A case with negative staining of phosphorylated ERK1/2 (p-ERK1/2).

Table 2 Association between *KRAS/BRAF* mutational status and clinicopathological factors in patients with ovarian cancer

		KRAS/BRAF mutation		
Factors	**Patients**	**Negative**	**Positive**	***P*-value**
FIGO stage				
I, II	18	8	10	<0.001
III, IV	38	38	2	
Grade				
G1	9	3	6	<0.001
G2, G3	49	43	6	
Histology				
Serous	28	26	2	0.014
Others	30	20	10	
Age (years)				
<60	35	28	7	0.293
⩾60	23	17	6	
p-ERK1/2				
Positive	27	15	12	<0.001
Negative	31	31	0	

FIGO, International Federation of Gynecology and Obstetrics; MAPK, mitogen-activated protein kinase; ERKV2, Extracellular signal-regulated protein kinases1/2.

lines were established in a *nu/nu* mouse model. All mice injected with CI-1040 developed significantly smaller intra-abdominal xenograft tumours than the mice carrying diluent control cells of the *KRAS* mutant cell line MADH2774 (Figure 7A). There were no differences in intra-abdominal xenograft tumour weights between the CI-1040-treated group and control groups transplanted with the wild-type *KRAS/BRAF* cell line SKOV3 (Figure 7B). Histological examination of the tumours after CI-1040 treatment showed inactivation of p-ERK1/2 in tumour cells based on immunohistochemistry (Figure 7C and D).

DISCUSSION

The significantly higher frequency of *KRAS/BRAF* mutations in non-serous type carcinomas compared with conventional high-grade serous carcinomas in this study is a finding of great interest. It suggests that conventional high-grade serous and non-serous tumours may be distinguished on the basis of characteristic genetic alterations. In addition, this observation further supports the theory that ovarian carcinoma arises from multiple pathways (Shih Ie and Kurman, 2004, 2005). In this model, conventional high-grade serous and non-serous carcinomas develop independently from one another and are characterised by different molecular genetic changes and gene expression profiles (Schwartz *et al*, 2002; Marquez *et al*, 2005).

We reported earlier that *KRAS* or *BRAF* mutations were quite common in low-grade serous ovarian carcinomas but rare in conventional high-grade serous carcinomas (Nakayama *et al*, 2006). Our present results showing low frequencies of either *KRAS* or *BRAF* mutations in conventional high-grade serous carcinoma are consistent with our earlier reports (Nakayama *et al*, 2006).

V600E is the most common *BRAF* mutation in ovarian cancer (Singer *et al*, 2003; Sieben *et al*, 2004; Shih Ie and Kurman, 2005; Nakayama *et al*, 2006). However, mutations at E585K and G463E have also been reported in ovarian cancer samples and cell lines (Davies *et al*, 2002). Therefore, further studies are needed to clarify the effects of other *BRAF* mutations in ovarian cancer, and to completely describe the mutation profile of *KRAS-BRAF* signalling in established ovarian cancer cell lines.

In this study, we also showed that the ERK–MAPK pathway was activated in 15 (33.3%) out of 45 ovarian carcinomas and activation depended on the mutational status of *KRAS* and *BRAF*. This is in contrast with a recent report showing that this pathway is frequently activated independent of the status of *KRAS* and *BRAF* in endometrioid-type endometrial cancer (Mizumoto *et al*, 2007). This discrepancy may be because of differences in organ-specific oncogenic pathways. The RAS–RAF–MEK–ERK pathway may play an important role in ovarian carcinogenesis but not in endometrial carcinogenesis. Similarly, alternative pathways for ERK activation, such as crosstalk with the PI3K pathway, exist in endometrial cancer but are rare in ovarian cancer. Indeed, PI3K signalling by either *PIK3CA* or *PTEN* mutations occurs in 40% of endometrial cancers but in <5% of ovarian cancers (Tashiro *et al*, 1997; Oda *et al*, 2005; Kolasa *et al*, 2006; Nakayama *et al*, 2006).

In this study, *KRAS* /*BRAF* mutations tended to have a favourable but not statistically significant effect on overall survival. Our findings contrast with a recent report showing a positive correlation between a *KRAS* or *BRAF* mutation and clinical aggressiveness in colorectal, non-small-cell lung, and thyroid cancers (Lievre *et al*, 2006; Lee *et al*, 2007; Massarelli *et al*, 2007). This difference in prognostic significance between ovarian cancer and the latter types is intriguing, and it probably reflects organ-specific roles of the *KRAS/BRAF* pathway. In this study, 8 out of 9 *KRAS/BRAF* mutations were identified in early stage (stage I, II) tumours. This may reflect a more indolent course of tumours with *KRAS/BRAF* mutations.

In an earlier report, advanced ovarian cancer patients (stage III, IV) with p-ERK expression had a longer overall survival than patients with low p-ERK values (Hsu *et al*, 2004). However, we did not find a significant correlation between p-ERK expression and overall survival in our study. This difference may be because of a

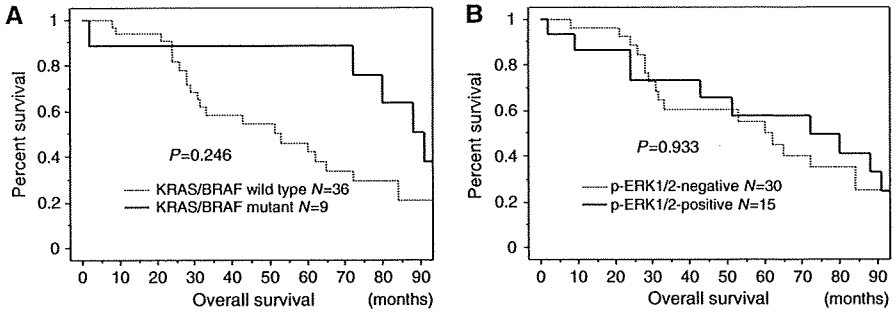

Figure 3 Kaplan–Meier survival curve in 45 patients with ovarian carcinoma according to *KRAS/BRAF* mutation and phosphorylated ERK (p-ERK) expression. (**A**) KRAS/BRAF mutational status correlates with favourable overall survival in patients with ovarian carcinoma. (**B**) p-ERK1/2 expression does not correlate with shorter overall survival in patients with ovarian carcinoma.

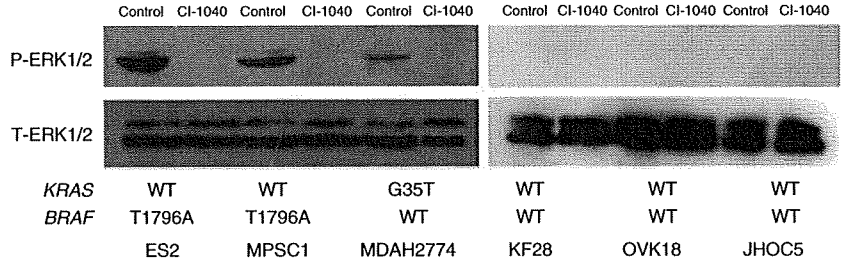

Figure 4 Western blot analysis. Expression of phosphorylated ERK1/2 (p-ERK1/2) is undetectable in all CI-1040-treated samples. A similar amount of protein was loaded in CI-1040 and DMSO-treated samples as evidenced by a similar intensity of total ERK1/2. D, DMSO treatment, C, and CI-1040 treatment.

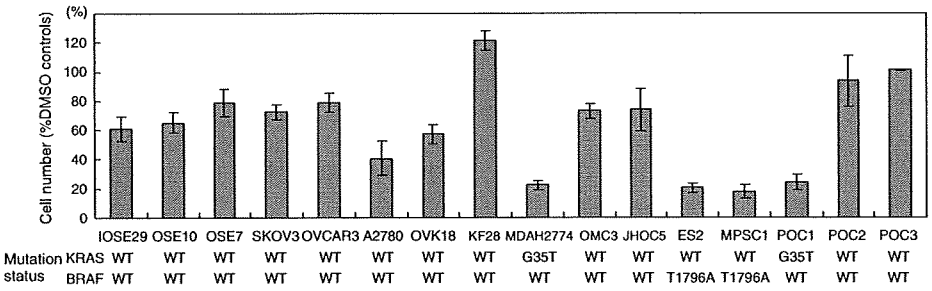

Figure 5 Effects of CI-1040 on cell proliferation. Cells were counted after 72 h of CI-1040 or DMSO (control) treatment. The mutational status of *KRAS* and *BRAF* for each sample is shown under the cell lines and primary cancer cell cultures. Ovarian cancers with mutations in either *KRAS* or *BRAF* are more sensitive to growth inhibition by CI-1040 than those with wild-type (WT) sequences.

higher percentage of early-stage ovarian cancers and endometrioid and mucinous histology tumours being included in this study as compared with the earlier study.

Although the biological roles of the RAS–RAF–MEK–ERK pathways in human cancer have been thoroughly investigated, there have been no recent studies. Therefore, it is not known whether the activation of *KRAS* or *BRAF* mutations alters the effects of these pathways on tumour progression. In this study, we carried out a genotype–phenotype correlation of ovarian cancer cells using a MEK inhibitor, CI-1040. In this study, we focussed on CI-1040 because it inhibited the common downstream target in the RAS signalling pathway. Therefore, CI-1040 has the potential to be developed into a drug for the treatment of ovarian carcinomas in patients with either *KRAS* or *BRAF* mutations. An oral formulation of CI-1040 had already been shown to be an effective MEK inhibitor and was generally well tolerated in a multicentre phase II study (Rinehart *et al*, 2004). Our results provide compelling evidence that the biological effects of the ERK signalling pathway depend on the mutational status of its upstream regulators, (i.e.), the *KRAS* and *BRAF* genes. Ovarian carcinomas with mutations in either *KRAS* or *BRAF* were more sensitive to growth inhibition and apoptosis induction by the MEK inhibitor, CI-1040. This observation suggests that ovarian carcinomas with mutations in either *KRAS* or *BRAF* are more highly dependent on the activation of the RAS–RAF–MEK–ERK pathway for cell proliferation and survival than those without such mutations. Thus, inactivation of ERK1/2 results in marked growth inhibition in ovarian carcinomas with mutations in *KRAS* or *BRAF* in comparison with only a modest effect on wild-type tumours. The above observations lend strong support to the view of 'kinase addiction' by which the activating mutations in the kinase pathway confer susceptibility of the tumours to an inhibitor (Sebolt-Leopold *et al*, 1999; Arteaga and Baselga, 2004). In microsatellite-unstable colorectal cancer cell lines, the effect of BRAF inhibition depended on whether the cell harboured a *BRAF* or a *KRAS* mutation. *BRAF* inhibition by small interfering RNA resulted in significantly decreased proliferation and increased apoptosis in the *BRAF* mutant lines. In contrast, this effect was not seen in the *KRAS* mutant lines (Preto *et al*, 2008). Cells carrying *BRAF* mutations have also been shown to be more sensitive to

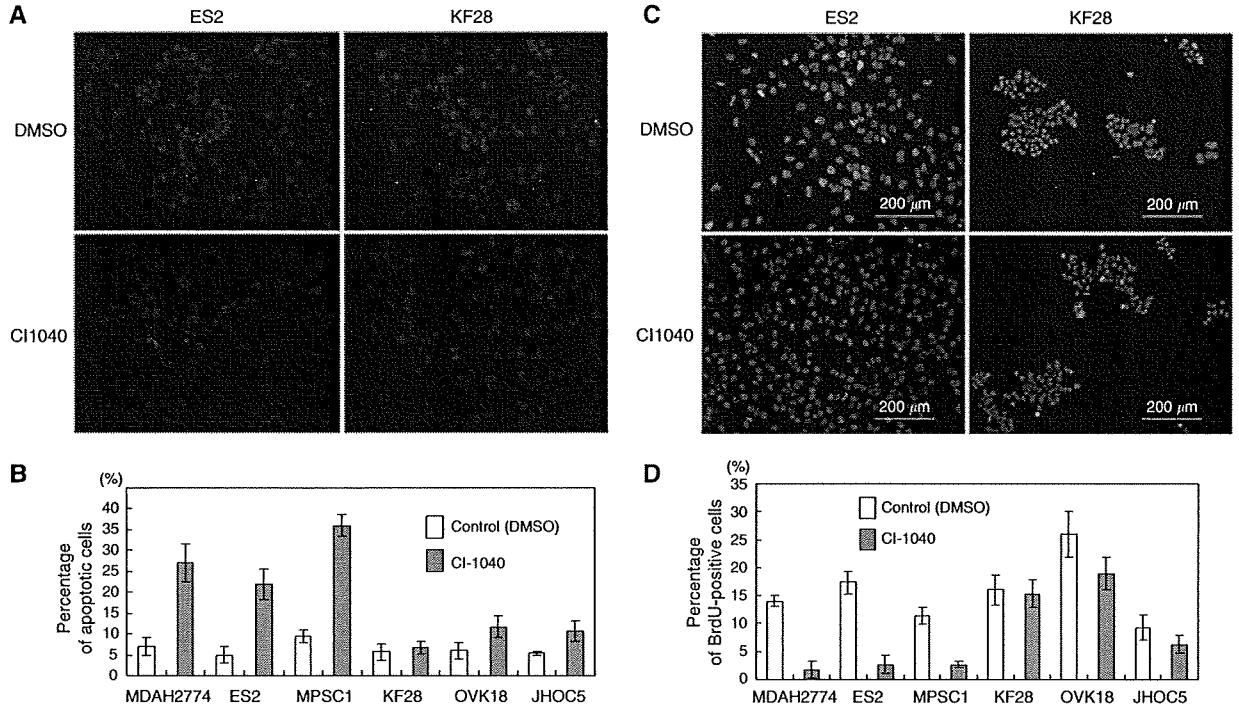

Figure 6 Detection of apoptotic cells and proliferation cells. (**A**) The CI-1040-treated ES2 cells, but not KF28 cells, show morphological features typical of apoptosis. (**B**) Apoptotic cells are quantified by counting them under a fluorescent microscope. (**C**) Treatment with CI-1040 decreases DNA synthesis as measured by BrdUrd uptake in ES2 cells, but not KF28 cells. (**D**) Proliferation is estimated by counting BrdUrd-stained cells under a fluorescent microscope. The experiment was performed 72 h after CI-1040 or DMSO treatment.

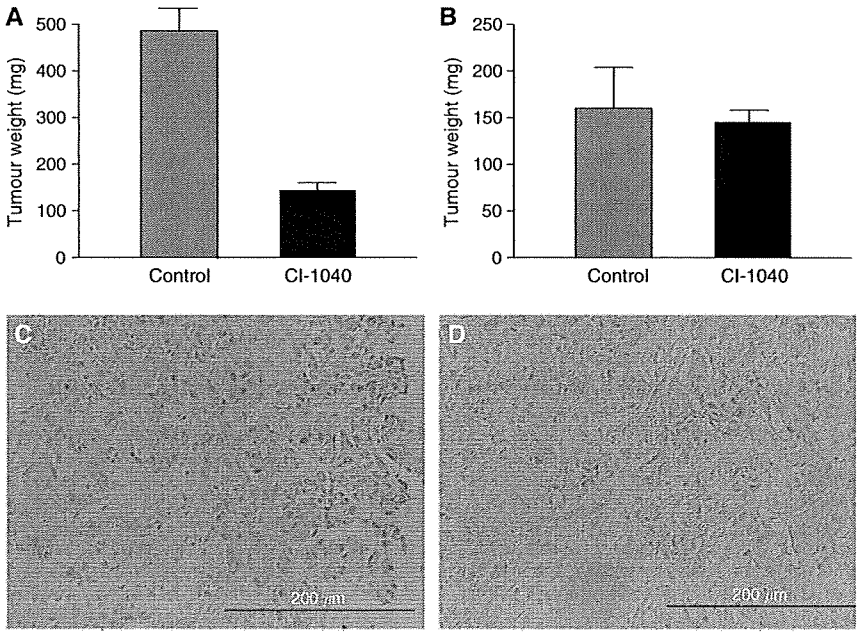

Figure 7 Effects of CI-1040 in a mouse xenograft model. (**A**) CI-1040-treated cells produced small tumour nodules in the peritoneal cavity. However, the diluent control-treated cells grew much larger i.p. tumours in *KRAS* mutant MDAH2774 cells. (**B**) In contrast, there were no differences in tumour weights between CI-1040-treated cells and control-treated cells in wild-type (WT) *KRAS/BRAF* SKOV3 cells. Tumours were excised and weighed. The data are expressed as the total tumour weight from each mouse. (**C** and **D**) Immunohistochemical staining of phosphorylated extracellular-regulated kinase 1/2 (p-ERK1/2) in tumours with *KRAS* mutant MDAH2774 cells. (**C**) Intense immunoreactivity is present in both the nucleus and the cytoplasm in CI-1040-untreated tumour. (**D**) Immunoreactivity is absent in both the nucleus and the cytoplasm in CI-1040-untreated tumour cells.

MEK inhibitors than cells with *RAS* mutations (Solit *et al*, 2006). This raises the possibility that *KRAS* and *BRAF* mutant cancer cells might be differentially dependent on signalling mechanisms that involve MEK. This difference in sensitivity to the RAS–RAF–MEK–ERK pathway between ovarian cancer and the latter types is intriguing, and it probably reflects organ-specific roles of the *KRAS and BRAF* oncogenes.

In light of our *in vivo* and *in vitro* findings, we propose that ovarian cancer patients with *KRAS* or *BRAF* mutations be considered for MEK inhibitor (CI-1040) therapy if they recur after conventional platinum and taxane chemotherapy.

Thus far, the MEK inhibitor CI-1040 has fared poorly in clinical trials for breast, colon, and lung cancer (Rinehart *et al*, 2004). However, its favourable therapeutic index and high selectivity may outweigh its shortcomings in *KRAS* and *BRAF* mutant ovarian cancer. Therefore, we recommend that in further clinical trials of MEK inhibitors for ovarian cancer, patients are stratified on the basis of *KRAS/BRAF* mutational status.

In summary, we have shown that the phenotypic change in ovarian carcinomas in response to ERK1/2 inactivation depends on the mutational status of *KRAS and BRAF*. The findings in this study provide new insight into the biological roles of the RAS–RAF–MEK–ERK signalling pathway in ovarian carcinomas. In addition, our observations have an important therapeutic implication in ovarian cancer patients with *KRAS* or *BRAF* mutations. Ovarian carcinomas with *KRAS* or *BRAF* mutation are clinically low-grade carcinomas of serous or other histological subtypes that are often refractory to conventional cytotoxic chemotherapy (Bristow *et al*, 2002a, b; Winter *et al*, 2007). Therefore, detection of *KRAS* and *BRAF* mutations in ovarian cancers may identify patients who will benefit from CI-1040 therapy.

ACKNOWLEDGEMENTS

This study is supported by grants from the Ministry of Education, Culture, Sports, Science and Technology in Japan, and the Japan Society of Gynecologic Oncology.

Supplementary Information accompanies the paper on British Journal of Cancer website (http://www.nature.com/bjc)

Translational Therapeutics

REFERENCES

Allen LF, Sebolt-Leopold J, Meyer MB (2003) CI-1040 (PD184352), a targeted signal transduction inhibitor of MEK (MAPKK). *Semin Oncol* **30:** 105–116

Arteaga CL, Baselga J (2004) Tyrosine kinase inhibitors: why does the current process of clinical development not apply to them? *Cancer Cell* **5:** 525–531

Bristow RE, Gossett DR, Shook DR, Zahurak ML, Tomacruz RS, Armstrong DK, Montz FJ (2002a) Micropapillary serous ovarian carcinoma: surgical management and clinical outcome. *Gynecol Oncol* **86:** 163–170

Bristow RE, Gossett DR, Shook DR, Zahurak ML, Tomacruz RS, Armstrong DK, Montz FJ (2002b) Recurrent micropapillary serous ovarian carcinoma. *Cancer* **95:** 791–800

Brose MS, Volpe P, Feldman M, Kumar M, Rishi I, Gerrero R, Einhorn E, Herlyn M, Minna J, Nicholson A, Roth JA, Albelda SM, Davies H, Cox C, Brignell G, Stephens P, Futreal PA, Wooster R, Stratton MR, Weber BL (2002) BRAF and RAS mutations in human lung cancer and melanoma. *Cancer Res* **62:** 6997–7000

Davies H, Bignell GR, Cox C, Stephens P, Edkins S, Clegg S, Teague J, Woffendin H, Garnett MJ, Bottomley W, Davis N, Dicks E, Ewing R, Floyd Y, Gray K, Hall S, Hawes R, Hughes J, Kosmidou V, Menzies A, Mould C, Parker A, Stevens C, Watt S, Hooper S, Wilson R, Jayatilake H, Gusterson BA, Cooper C, Shipley J, Hargrave D, Pritchard-Jones K, Maitland N, Chenevix-Trench G, Riggins GJ, Bigner DD, Palmieri G, Cossu A, Flanagan A, Nicholson A, Ho JW, Leung SY, Yuen ST, Weber BL, Seigler HF, Darrow TL, Paterson H, Marais R, Marshall CJ, Wooster R, Stratton MR, Futreal PA (2002) Mutations of the BRAF gene in human cancer. *Nature* **417:** 949–954

Gorden A, Osman I, Gai W, He D, Huang W, Davidson A, Houghton AN, Busam K, Polsky D (2003) Analysis of BRAF and N-RAS mutations in metastatic melanoma tissues. *Cancer Res* **63:** 3955–3957

Hsu CY, Bristow R, Cha MS, Wang BG, Ho CL, Kurman RJ, Wang TL, Shih Ie M (2004) Characterization of active mitogen-activated protein kinase in ovarian serous carcinomas. *Clin Cancer Res* **10:** 6432–6436

Kolasa IK, Rembiszewska A, Janiec-Jankowska A, Dansonka-Mieszkowska A, Lewandowska AM, Konopka B, Kupryjanczyk J (2006) PTEN mutation, expression and LOH at its locus in ovarian carcinomas. Relation to TP53, K-RAS and BRCA1 mutations. *Gynecol Oncol* **103:** 692–697

Lee JH, Lee ES, Kim YS (2007) Clinicopathologic significance of BRAF V600E mutation in papillary carcinomas of the thyroid: a meta-analysis. *Cancer* **110:** 38–46

Lievre A, Bachet JB, Le Corre D, Boige V, Landi B, Emile JF, Cote JF, Tomasic G, Penna C, Ducreux M, Rougier P, Penault-Llorca F, Laurent-Puig P (2006) KRAS mutation status is predictive of response to cetuximab therapy in colorectal cancer. *Cancer Res* **66:** 3992–3995

Marquez RT, Baggerly KA, Patterson AP, Liu J, Broaddus R, Frumovitz M, Atkinson EN, Smith DI, Hartmann L, Fishman D, Berchuck A, Whitaker R, Gershenson DM, Mills GB, Bast Jr RC, Lu KH (2005) Patterns of gene expression in different histotypes of epithelial ovarian cancer correlate with those in normal fallopian tube, endometrium, and colon. *Clin Cancer Res* **11:** 6116–6126

Massarelli E, Varella-Garcia M, Tang X, Xavier AC, Ozburn NC, Liu DD, Bekele BN, Herbst RS, Wistuba II (2007) KRAS mutation is an important predictor of resistance to therapy with epidermal growth factor receptor tyrosine kinase inhibitors in non-small-cell lung cancer. *Clin Cancer Res* **13:** 2890–2896

Mizumoto Y, Kyo S, Mori N, Sakaguchi J, Ohno S, Maida Y, Hashimoto M, Takakura M, Inoue M (2007) Activation of ERK1/2 occurs independently of KRAS or BRAF status in endometrial cancer and is associated with favorable prognosis. *Cancer Sci* **98:** 652–658

Nakayama K, Miyazaki K, Kanzaki A, Fukumoto M, Takebayashi Y (2001) Expression and cisplatin sensitivity of copper-transporting P-type adenosine triphosphatase (ATP7B) in human solid carcinoma cell lines. *Oncol Rep* **8:** 1285–1287

Nakayama K, Nakayama N, Kurman RJ, Cope L, Pohl G, Samuels Y, Velculescu VE, Wang TL, Shih Ie M (2006) Sequence mutations and amplification of PIK3CA and AKT2 genes in purified ovarian serous neoplasms. *Cancer Biol Ther* **5:** 779–785

Oda K, Stokoe D, Taketani Y, McCormick F (2005) High frequency of coexistent mutations of PIK3CA and PTEN genes in endometrial carcinoma. *Cancer Res* **65:** 10669–10673

Oliveira C, Velho S, Moutinho C, Ferreira A, Preto A, Domingo E, Capelinha AP, Duval A, Hamelin R, Machado JC, Schwartz Jr S, Carneiro F, Seruca R (2007) KRAS and BRAF oncogenic mutations in MSS colorectal carcinoma progression. *Oncogene* **26:** 158–163

Olson JM, Hallahan AR (2004) p38 MAP kinase: a convergence point in cancer therapy. *Trends Mol Med* **10:** 125–129

Peyssonnaux C, Eychene A (2001) The Raf/MEK/ERK pathway: new concepts of activation. *Biol Cell* **93:** 53–62

Pohl G, Ho CL, Kurman RJ, Bristow R, Wang TL, Shih Ie M (2005) Inactivation of the mitogen-activated protein kinase pathway as a potential target-based therapy in ovarian serous tumors with KRAS or BRAF mutations. *Cancer Res* **65:** 1994–2000

Preto A, Figueiredo J, Velho S, Ribeiro AS, Soares P, Oliveira C, Seruca R (2008) BRAF provides proliferation and survival signals in MSI colorectal carcinoma cells displaying BRAF(V600E) but not KRAS mutations. *J Pathol* **214:** 320–327

Rinehart J, Adjei AA, Lorusso PM, Waterhouse D, Hecht JR, Natale RB, Hamid O, Varterasian M, Asbury P, Kaldjian EP, Gulyas S, Mitchell DY, Herrera R, Sebolt-Leopold JS, Meyer MB (2004) Multicenter phase II study of the oral MEK inhibitor, CI-1040, in patients with advanced non-small-cell lung, breast, colon, and pancreatic cancer. *J Clin Oncol* **22:** 4456–4462

Schaeffer HJ, Weber MJ (1999) Mitogen-activated protein kinases: specific messages from ubiquitous messengers. *Mol Cell Biol* **19:** 2435–2444

Schwartz DR, Kardia SL, Shedden KA, Kuick R, Michailidis G, Taylor JM, Misek DE, Wu R, Zhai Y, Darrah DM, Reed H, Ellenson LH, Giordano TJ, Fearon ER, Hanash SM, Cho KR (2002) Gene expression in ovarian cancer reflects both morphology and biological behavior, distinguishing clear cell from other poor-prognosis ovarian carcinomas. *Cancer Res* **62:** 4722–4729

Sebolt-Leopold JS (2004) MEK inhibitors: a therapeutic approach to targeting the Ras-MAP kinase pathway in tumors. *Curr Pharm Des* **10:** 1907–1914

Sebolt-Leopold JS, Dudley DT, Herrera R, Van Becelaere K, Wiland A, Gowan RC, Tecle H, Barrett SD, Bridges A, Przybranowski S, Leopold WR, Saltiel AR (1999) Blockade of the MAP kinase pathway suppresses growth of colon tumors *in vivo*. *Nat Med* **5:** 810–816

Sebolt-Leopold JS, Van Becelaere K, Hook K, Herrera R (2003) Biomarker assays for phosphorylated MAP kinase. Their utility for measurement of MEK inhibition. *Methods Mol Med* **85:** 31–38

Shih Ie M, Kurman RJ (2004) Ovarian tumorigenesis: a proposed model based on morphological and molecular genetic analysis. *Am J Pathol* **164:** 1511–1518

Shih Ie M, Kurman RJ (2005) Molecular pathogenesis of ovarian borderline tumors: new insights and old challenges. *Clin Cancer Res* **11:** 7273–7279

Sieben NL, Macropoulos P, Roemen GM, Kolkman-Uljee SM, Jan Fleuren G, Houmadi R, Diss T, Warren B, Al Adnani M, De Goeij AP, Krausz T, Flanagan AM (2004) In ovarian neoplasms, BRAF, but not KRAS, mutations are restricted to low-grade serous tumours. *J Pathol* **202:** 336–340

Singer G, Kurman RJ, Chang HW, Cho SK, Shih Ie M (2002) Diverse tumorigenic pathways in ovarian serous carcinoma. *Am J Pathol* **160:** 1223–1228

Singer G, Oldt III R, Cohen Y, Wang BG, Sidransky D, Kurman RJ, Shih Ie M (2003) Mutations in BRAF and KRAS characterize the development of low-grade ovarian serous carcinoma. *J Natl Cancer Inst* **95:** 484–486

Solit DB, Garraway LA, Pratilas CA, Sawai A, Getz G, Basso A, Ye Q, Lobo JM, She Y, Osman I, Golub TR, Sebolt-Leopold J, Sellers WR, Rosen N (2006) BRAF mutation predicts sensitivity to MEK inhibition. *Nature* **439:** 358–362

Tashiro H, Blazes MS, Wu R, Cho KR, Bose S, Wang SI, Li J, Parsons R, Ellenson LH (1997) Mutations in PTEN are frequent in endometrial carcinoma but rare in other common gynecological malignancies. *Cancer Res* **57:** 3935–3940

Wan PT, Garnett MJ, Roe SM, Lee S, Niculescu-Duvaz D, Good VM, Jones CM, Marshall CJ, Springer CJ, Barford D, Marais R (2004) Mechanism of activation of the RAF-ERK signaling pathway by oncogenic mutations of B-RAF. *Cell* **116:** 855–867

Wingo PA, Tong T, Bolden S (1995) Cancer statistics, 1995. *CA Cancer J Clin* **45:** 8–30

Winter III WE, Maxwell GL, Tian C, Carlson JW, Ozols RF, Rose PG, Markman M, Armstrong DK, Muggia F, McGuire WP (2007) Prognostic factors for stage III epithelial ovarian cancer: a Gynecologic Oncology Group Study. *J Clin Oncol* **25:** 3621–3627

Workman P (1998) United Kingdom Co-ordinating Committee on Cancer Research (UKCCCR) Guidelines for the Welfare of Animals in Experimental Neoplasia (Second Edition). *Br J Cancer* **77:** 1–10

Yamamoto K, Kikuchi Y, Kudoh K, Nagata I (2000) Modulation of cisplatin sensitivity by taxol in cisplatin-sensitive and -resistant human ovarian carcinoma cell lines. *J Cancer Res Clin Oncol* **126:** 168–172

Applied Radiation and Isotopes 67 (2009) 155–159

Contents lists available at ScienceDirect

Applied Radiation and Isotopes

journal homepage: www.elsevier.com/locate/apradiso

Spectromicroscopic film dosimetry for high-energy microbeam from synchrotron radiation

Nobuteru Nariyama [a,*], Takuji Ohigashi [a,1], Keiji Umetani [a], Kunio Shinohara [a,2], Hiroki Tanaka [b], Akira Maruhashi [b], Genro Kashino [b], Ai Kurihara [c], Takeshi Kondob [d], Manabu Fukumoto [c], Koji Ono [b]

[a] Japan Synchrotron Radiation Research Institute, Kouto 1-1-1, Sayo, Hyogo 679-5198, Japan
[b] Research Reactor Institute, Kyoto University, Kumatori, Sennan, Osaka 590-0494, Japan
[c] Institute of Development, Aging and Cancer, Tohoku University, Seiryo, Aoba, Sendai, Miyagi 980-8575, Japan
[d] Kobe University, Graduate School of Medicine, Kusunoki, Chuo, Kobe, Hyogo 650-0017, Japan

ARTICLE INFO

Article history:
Received 7 April 2008
Received in revised form
19 May 2008
Accepted 1 August 2008

Keywords:
GafChromic film
Dose
Microbeam
Synchrotron radiation
PENELOPE

ABSTRACT

A microscope with band-pass filters was used to measure the optical-density distribution of GafChromic films irradiated with multi-slit microbeam X-rays. The planar width was 25 μm, and the center-to-center distance was 200 μm. The peak and valley dose rates in air were found to be 120 and 0.7 Gy/s, respectively. In a polymethylmethacrylate phantom, the peak-to-valley dose ratio decreased to 80 at a 1-mm depth. Doses calculated with the PENELOPE code agreed with those around the peak but became smaller in the valley.

1. Introduction

The use of a high-energy synchrotron-radiation microbeam produced through a multi-slit collimator has been reported to enhance the tolerance of normal tissue to radiation (Slatkin et al., 1992, 1995), and clinical microbeam radiation therapy (MRT) has been studied intensively in recent years (Laissue et al., 1998; Dilmanian et al., 2002; Bräuer-Krisch et al., 2005). The treatment results in extended median survival time (Laissue et al., 1998), depending on the valley dose between the peaks (Dilmanian et al., 2002). In this context, the recovery of normal tissue in the peak depends on the dose in the valley as well as that in the peak. The width of the peak region was 20–25 μm, and the spacing between the regions was 100–300 μm. Thus, it is important to examine the dose distribution with micro-scale resolution in order to clarify this phenomenon.

The method for achieving such clarification, however, has not yet been established because there has been no demand for it. GafChromic radiochromic film (American Association of Physicists in Medicine (AAPM), 1998) appears to be a rare promising candidate for such an application, because the spatial resolution has been reported to be 0.8 μm (McLaughlin et al., 1991), and in fact this film has been used for the evaluation of dose distribution with micrometer spatial resolution utilizing a microdensitometer (Lee et al., 2004; Bräuer-Krisch et al., 2005). Here it should be noted that although an image with excellent resolution can certainly be obtained using a microscope or microdensitometer, there remained an ambiguity without a quantitative estimation whether the optical density (OD) obtained from the observed image exactly reflected the dose in the area; therefore, a quantitative estimation was necessary. An effective method of checking the peak dose was by comparison with the dose of the broad beam, because the photons were incident directly on the area, and the difference would be explained basically by the beam size effect, which is described later.

A basic problem of the microdosimetric measurement of GafChromic film is that the intensity of transparent light through the smaller area becomes weaker and the signal fluctuates greatly. The uniformity of the film also becomes worse. To enhance measurement accuracy, we used a linear relation of OD versus dose, which is achieved by using monochromatic light for the OD measurement. We also paid attention to the calibration; films should be irradiated with X-rays with the same energy as the microbeam at calibration.

* Corresponding author.
E-mail address: nariyama@spring8.or.jp (N. Nariyama).
[1] Present address: Research Organization of Science and Engineering, Ritsumeikan University, 1-1-1 Noji Higashi, Kusatsu, Shiga 525-8577, Japan.
[2] Present address: Advanced Research Institute for Science and Engineering, Waseda University, Okubo, Shinjuku, Tokyo 169-8555, Japan.

0969-8043/$ - see front matter © 2008 Elsevier Ltd. All rights reserved.
doi:10.1016/j.apradiso.2008.08.002

For the analysis of the localized irradiation, a Monte Carlo simulation is useful. General-purpose Monte Carlo codes adopt a "condensed" simulation algorithm for electron transport, which uses multiple-scattering theory instead of following the single scattering. This simulation occasionally breaks down when a small step length is used for low-Z material (Nariyama, 1995). On the other hand, a PENELOPE code (Salvat et al., 2006) adopts a mixed simulation of hard and soft interactions that depends on the scattering angle and energy loss. In the hard collision, single scattering is followed, and in the soft collision multiple-scattering theory is used, which agrees with the Goudsmitt–Saunders theory. When analyzing the dose distribution for the microbeam, a spatial resolution of 1 μm is necessary, so that a small step length cannot be avoided in low-Z material for a "condensed" simulation. From this situation, the PENELOPE code was considered to be preferable for the present simulation.

In this study, optical microscopy was used to measure the OD distribution of the GafChromic film HD-810 irradiated with a multi-slit microbeam. To obtain linearity between the OD and dose in order to enhance the accuracy, we used band-pass filters. The films were calibrated in the same X-ray field, in which the air kerma of the broad beam was measured with a free-air ionization chamber, and the dose for the broad beam was compared with the peak dose for the evaluation of the micro-scale dose distribution measuring system. The peak and valley doses were compared with the results of Monte Carlo simulations.

2. Materials and methods

2.1. Microscopic dosimetry method

The base of the OD reader was a Nikon Eclipse 80i microscope, in which fly-eye lenses were used to homogenize the light intensity in the view. The magnification of the object lens was 20, and the numerical aperture (NA) was 0.45; the optical resolution was 0.9 μm, which was sufficient for the present measurement. To stabilize the light intensity, we connected the battery of the halogen lamp to an AC regulator, which brought the stability to within 0.4%. The light emitted from the lamp was monochromatized through a band-pass filter, and the light image passing the film was taken with a CCD camera, the RETIGA Exi, with a 12-bit gray scale. The image was 1392 × 1040 pixels with a pixel size of 6.45 μm. The image obtained was analyzed with Image Pro Plus software, and the brightness was converted to OD with the position information. The film was also scanned with an X–Y electric-powered stage.

During the series of measurements, including calibrations, the microscope was set in a dark room, and none of the optical conditions were changed because the OD significantly depended on the condition of the aperture stop and the view diaphragm, in addition to the lamp intensity. Homogeneous intensity of view, which was important for the present OD distribution measurements, was confirmed by measuring the light intensity distribution without the films.

The HD-810 (ISP Technologies Inc.) has two peaks in the absorption spectra: the largest absorbance, around 670 nm, was preferable for low-dose imaging, and the other absorbance, near 610 nm, was suitable for high-dose imaging. As a result, 601 and 668 nm wavelengths were used for the peak and valley doses, respectively. The full-width at half-maximum (FWHM) of the band-pass filters used were 8 and 7.5 nm for 601 and 668 nm, respectively.

In the configuration of the HD-810, the radiation-sensitive layer was only 6.5 μm thick, which was sandwiched with a 0.75-μm-thick thin cover and 96.5-μm-thick polyester. From the NA of the optical lens, the depth of field was estimated to be 1.7 μm at 668 nm, which was short enough compared with the thickness of the radiation-sensitive layer. This means that the adjustment of the focal point does not affect the OD measurement.

2.2. Beamline experiment

The irradiation of GafChromic film was carried out at the No.1 hutch of the white X-ray bending-magnet beamline BL28B2 in SPring-8, an 8-GeV large-scale synchrotron-radiation facility in Japan. The photon beam was linear-polarized, with the electric vector included in the horizontal plane. A filter of 3-mm-thick copper was inserted in the beam to remove the low-energy component, of which the spectra were calculated with the SPECTRA code (Tanaka and Kitamura, 2001), shown in Fig. 1. The energies were mainly distributed between 50 and 200 keV, peaking around 90 keV. This result did not contradict the measured half-value layer (HVL) in Cu of 2.2 mm, indicated in Table 1. In the energy region, the response of the HD-810 was almost constant (Nariyama, 2005). A non-uniform intensity distribution existed in the vertical direction of the beam, but the intensity was almost homogeneous in the horizontal direction. At the microbeam irradiations, the height was set to 3 mm in the homogeneous region.

The air kerma rate of the broad beam was measured with a free-air parallel-plate ionization chamber at an 85-mm gap (Nariyama et al., 2004). The electron escape fraction up to 300 keV was calculated with Monte Carlo transport code EGS4, considering the influence of linear polarization on the emission angle of photons and electrons (Nariyama et al., 1995). Fig. 1 indicates that above 200 keV the fraction was less than 5%, which was sufficiently low. Below 150 keV, the fraction had already been

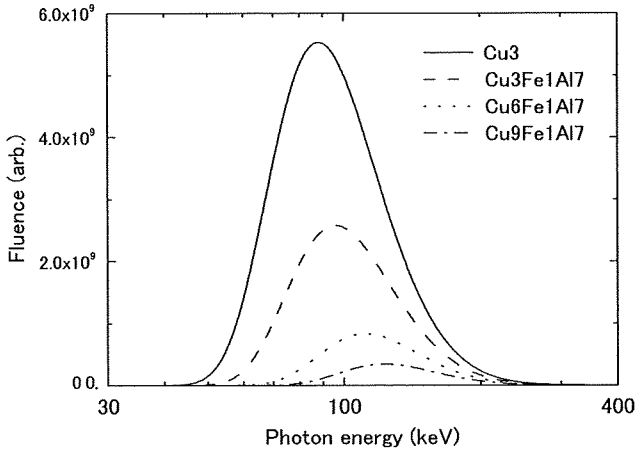

Fig. 1. Photon fluence calculated with SPECTRA code for various filters; each filter corresponds to that indicated in Table 1. The peak energies shifted from 90 keV to 95, 110 and 123 keV, respectively, with increasing filter thickness.

Table 1
Measured HVL and air kerma rate for a filtered beam at BL28B2

Filtration (mm)			HVL (mm Cu)	Air kerma rate (Gy/s)
Al	Fe	Cu		
0	0	3	2.20	150
7	1	3	2.47	80
7	1	6	3.20	36
7	1	9	–	19

confirmed experimentally (Nariyama et al., 1995). Using this ionization chamber, we measured the air kerma rate and found it to be 140–150 Gy/s, which slightly depended on the beam size because of the inhomogeneous strength distribution. The obtained values agreed with that of the HD-810 calibrated with ^{60}Co gamma rays considering the energy responses. When a voltage of 10 kV was applied, near saturation was attained.

A multi-slit collimator manufactured for microbeam production consisted of tungsten blocks, of which the thickness in the beam direction was 5 mm. Kapton films inserted in the slits maintained the spacing of 25 μm, and the center-to-center (c-t-c) distance between the Kapton areas was designed to be 200 μm. Two kinds of rotation stages and a *Z*-axis stage determined the collimator position and orientation. The slits were set to be aligned horizontally. The films were irradiated with the multi-slit microbeam through this collimator in free air and in a polymethylmethacrylate (PMMA) phantom of a 15-cm cube. In the air, the irradiation times were set to 1 and 10 s for the peak and valley areas, respectively, to optimize each OD. For the same reason, the time was set to 1–10 s in the phantom, depending on the positions of 0.1, 1, 3, 5 and 10 cm.

For reference, a single-slit collimator with a variable gap was also used. The material was 20-mm-thick tungsten. No solid material existed in the gap, which was electrically varied.

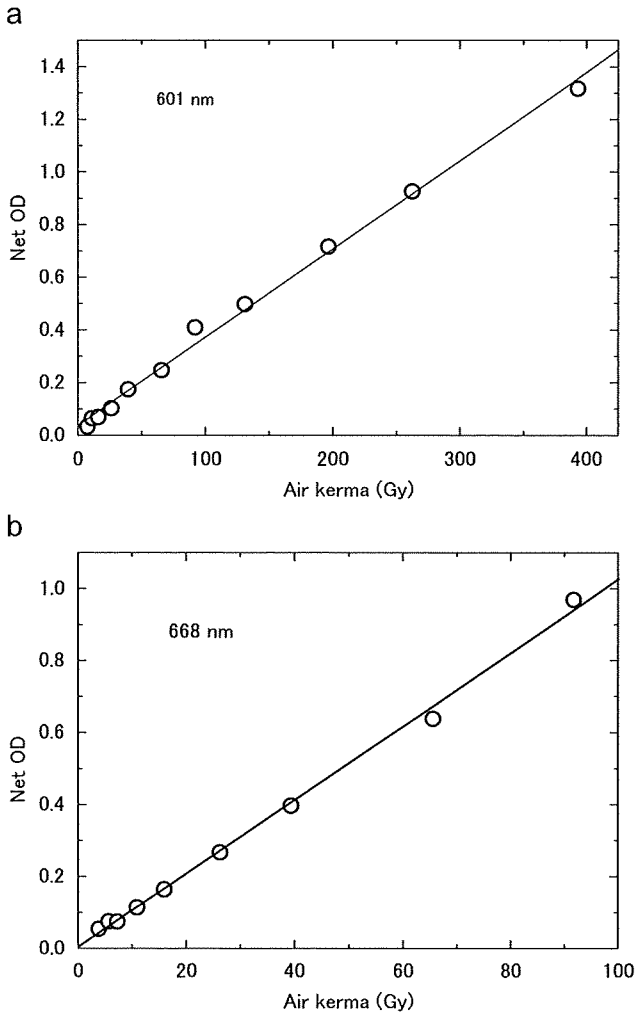

Fig. 2. Calibration curves of the HD-810: net OD versus air kerma at 601 and 668 nm.

2.3. Calibration method

The calibration of the HD-810 was also made at BL28B2 using the above-mentioned free-air ionization chamber. To vary the dose, we used a shutter fixed at the beamline, but the shortest available time was 0.2 s, so filters of Al, Fe and Cu in various thicknesses were added to lower the dose further. Table 1 summarizes the HVL of Cu and the air kerma rate for each filter combination, and Fig. 1 gives photon spectra calculated with SPECTRA; the spectra become harder with thickness, and the peak shifts up to 123 keV. The energy response of the HD-810 does not change considerably, so calibration of the HD-810 in these X-ray fields was possible. The irradiation doses were changed from 5 to 400 Gy, which yielded calibration curves at 601 and 668 nm, as shown in Fig. 2. In all repeated trials, we confirmed the linear relation between dose and OD. The beam size used was 1 mm in height by several mm in width.

In the present geometry of a beam size less than 1 mm, an electric equilibrium could not be achieved in air, even though sufficient distance was maintained. The only solution was to locate a solid in front of the radiation-sensitive material; here the films were irradiated on the reverse side, that is, the 96.5-μm polyester side, for all the calibrations and microbeam irradiations.

For the phantom, the dose in air was converted to a water dose using the mass energy-absorption coefficients; the ratio was 1.095 at 100 keV and 1.031 at 50 keV. For all the doses, a factor of 1.095 was used; even if the actual photon energies were lower than 100 keV, the overestimation of the conversion would be canceled because the energy response of the HD-810 decreased in the low-energy region.

2.4. Monte Carlo calculation

The dose distribution for the multi-slit beam was calculated with the PENELOPE code. A 0.1-mm-thick film was positioned at 50 cm behind the collimator consisting of tungsten and Kapton. In the PENMAIN program, the energies, positions and directions of the photon source were input as an IPSFN card; the energies were sampled using Fig. 1 and the incident angle was assumed to be parallel. Thus, the calculated energy deposition in the film was converted into those in air and water, respectively, using the ratios of the mass energy-absorption coefficients.

3. Results and discussion

3.1. Dose distribution for a multi-slit beam in air

Fig. 3 represents the result of the dose distribution in free air. The peak area was obtained at 601 nm from a film irradiated for 1 s, and the valley area at 668 nm from another film irradiated for 10 s. Both results were combined into one, so that some slight joints appeared around 10 Gy/s. The values were averaged in the longitudinal direction of the beam. The FWHM of the peak was 26–27 μm and the c–t–c distance was 200 μm, the same as designed. The peak and valley dose rates became 120 and 0.7 Gy/s, respectively, which led to a peak-to-valley dose ratio (PVDR) of 150.

The peak dose rate of 120 Gy/s, which was the dose rate in air, became smaller than 140–150 Gy/s in the broad beam. This was due to the lack of lateral electric equilibrium; the beam was so narrow that the region of electrons escaping to the outside could not be compensated for enough to become dominant. Fig. 4 shows the dose dependence on beam height, calculated with PENELOPE. The dose corresponded to that in the center of the water layer on

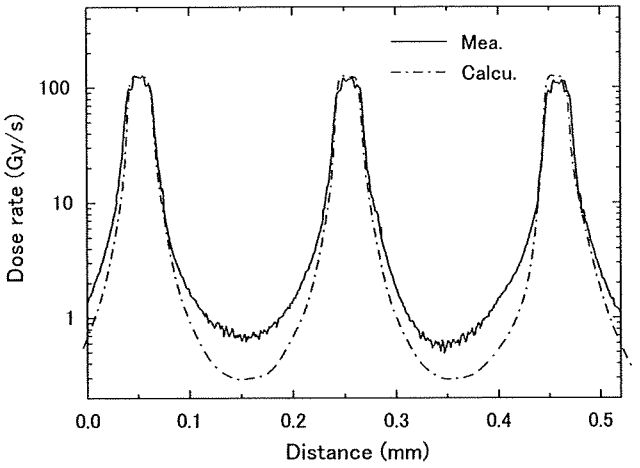

Fig. 3. Measured and calculated dose distribution in free air; both express the absolute values. The slits were aligned horizontally, and the vertical distribution was measured, averaged in the horizontal direction. While the peak doses agreed, the calculated valley doses became smaller than the measured doses.

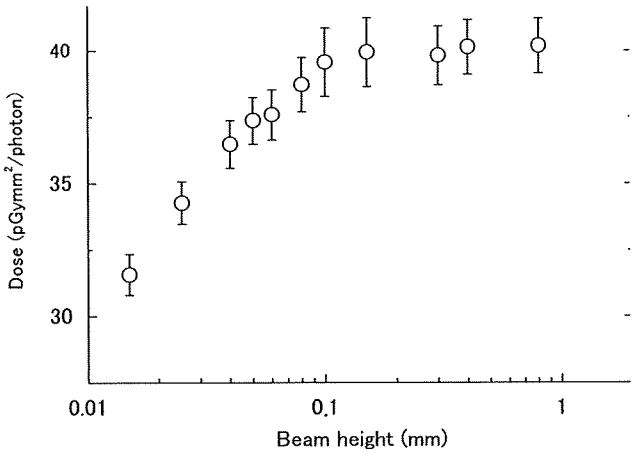

Fig. 4. Water doses calculated with PENELOPE as a function of beam height. The beam width was 1 mm, and the error bars express 3σ.

which the same photon beam of a 1-mm width passing through a 50-cm air layer was incident. In the figure, the dose started to decrease at a 100-μm height and became 85% at a 25-μm height. The length of 100 μm almost equaled the electron range at 100 keV in water, and the proportion of 85% agreed with the measured ratio of the peak dose to the broad-beam dose. The reliability of the dose for the broad beam was considered to be high because the conventional measuring method had been fully established. Thus, the assumption of lateral electric equilibrium succeeded in explaining the validity of the measured peak dose from the broad-beam dose.

Fig. 3 shows the result of the Monte Carlo calculations. The absolute dose was obtained as follows: the photon fluence necessary to obtain the dose of 150 Gy for a broad beam was calculated with PENELOPE using the energy spectra in Fig. 1. The doses per photon calculated with the code for a microbeam were then converted to the dose at the fluence. Thus the obtained values agreed with the measured values in the peak, but were smaller in the valley: 0.3 Gy/s. In Fig. 3, the calculated dose of the transmitted photons through the 5-mm-thick tungsten was only 0.04 Gy/s, which did not influence the valley dose.

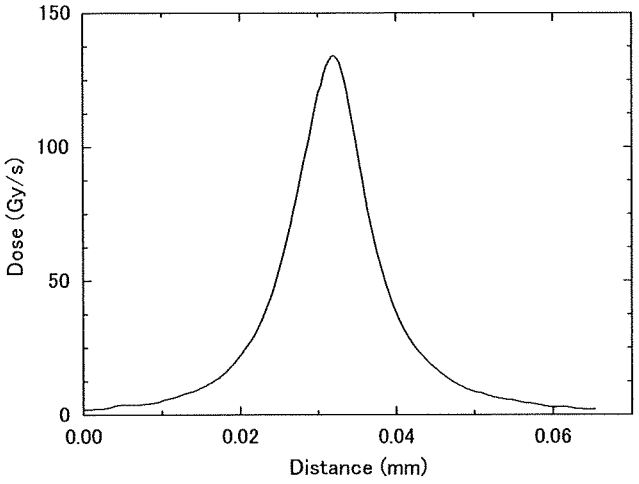

Fig. 5. Dose distribution measured with HD-810 for the single slit with a 14.5-μm gap. A smooth peaking curve was observed.

Fig. 3 depicts non-smooth distribution near the peak. On the other hand, for the single slit with a 14.5-μm gap, with no supporting material in the gap, the fluctuation clearly diminished as shown in Fig. 5. The contrast with Fig. 3 suggests that the supporting material of the stacked Kapton films affected the fine dose distribution. Dose attenuation in the 5-mm-thick Kapton was 5%. From a different point of view, the rough distribution in Fig. 3 demonstrated the high resolution of the present microscopic method.

A simulation for the single slit was also made, and smaller values were obtained at the foot. This phenomenon was the same as that obtained before (Siegbahn et al., 2005). One possible reason is that the physical model was not incorporated into the code. The synchrotron radiation is linearly polarized in the horizontal plane. The photons are scattered preferably in the vertical direction (Nariyama et al., 1995). In the present experimental setup, the slits were set to be aligned horizontally, so that the inclusion of the model may have raised the valley dose.

Scattering in the wall may be another reason. The valley dose rate occasionally changed from 0.7 to 0.9 Gy/s, depending on the orientation of the collimator. In the valley, the dose was not flat as shown in Fig. 3. Since the electron range at 100 keV is 143 μm, electrons can also play a considerable role in slope production. The simulation inevitably assumes geometrical factors such as the complete parallel orientation and smoothing of the collimator surface and the orientation of the collimator, although these are not known exactly. As for the orientation, the valley doses did not drop lower than 0.7 Gy/s, which suggests the condition under which the collimator pointed to the beam most directly.

3.2. Dose distribution in phantom

Fig. 6 gives the water-dose distribution at a 1-mm depth in the cubic PMMA phantom. The peak dose was 120 Gy/s, and the valley dose was 1.5–1.7 Gy/s; that is, the PVDR decreased to 77. At depths of 10- and 30-mm, the PVDR decreased slightly to 67. Thus, whereas the peak dose scarcely differed from that in free air, the valley dose increased because of the scattered photons in the phantom. The FWHM became 28–29 μm, slightly thicker than in air. This is also due to the scattered photons. While the calculated values of PENELOPE reproduced the shape above 5 Gy/s, in the valley the values became smaller, as in the air.

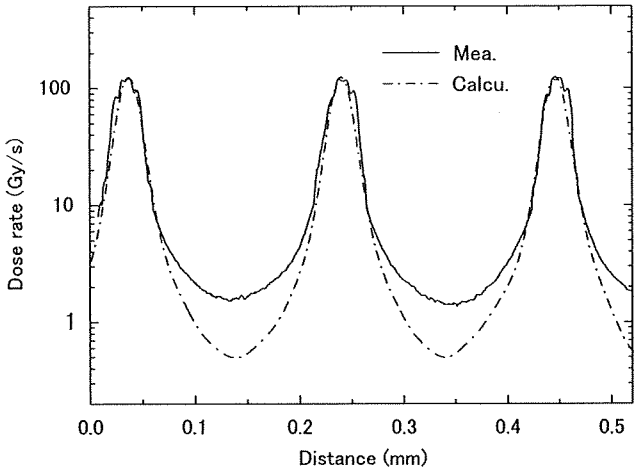

Fig. 6. Water-dose distribution measured and calculated at a 1-mm depth in the 15-cm-thick PMMA phantom. The peaks became thicker than in air, and the valley dose increased.

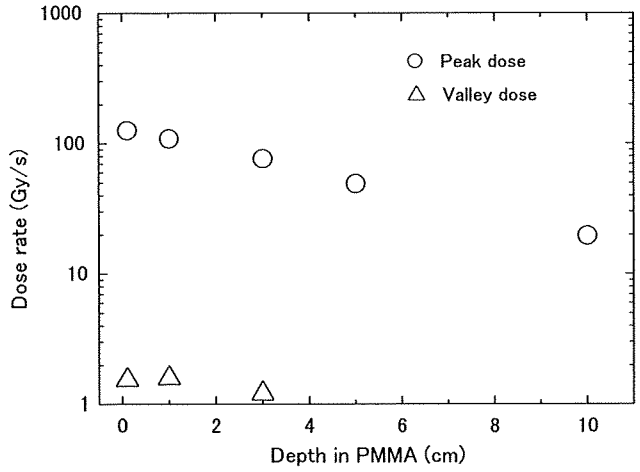

Fig. 7. Measured depth–dose curves in the peak and valley for the PMMA phantom.

Fig. 7 shows the depth–dose curve in the phantom at the peak and valley parts. Because of the narrow beam, the attenuation in the peak was approximately exponential, and the attenuation coefficient almost agreed with that in PMMA at 100 keV.

4. Conclusions

The peak dose with a 25-μm width, which was measured with a spectroscopic microscope, was confirmed by comparison with the broad-beam dose. The present measuring system employs a conventional microscope to which filters were added. The advantage of using a microscope is that one obtains a direct image, which can be processed with general-purpose image-processing software. This simple and fast measurement, with the latter feature important to avoid colorization, is superior to the use of a scanning-type microdensitometer. The disadvantage is the required two-time irradiation for the peak and valley. The lack of band-pass filters would expand the upper limit and enable one-time measurement at the cost of accuracy. When the slope between the peak and the valley is to be determined, the method described here is also preferable. With this flexibility, the present equipment should be applied to MRT and microbeam research.

Acknowledgement

The synchrotron-radiation experiments were performed at the BL28B2 in the SPring-8 with the approval of the Japan Synchrotron Radiation Research Institute (JASRI) (Proposal No. 2007A1214, 2007B1241).

References

American Association of Physicists in Medicine, 1998. Radiochromic film dosimetry. AAPM Report No. 63.

Bräuer-Krisch, E., Bravin, A., Zhang, L., Siegbahn, E., Stepanek, J., Blattmann, H., Slatkin, D.N., Gebbers, J.O., Jasmin, M., Laissue, J.A., 2005. Characterization of a tungsten/gas multislit collimator for microbeam radiation therapy at the European Synchrotron Radiation Facility. Rev. Sci. Instrum. 76, 064303.

Dilmanian, F.A., Button, T.M., Le Duc, G., Zhong, N., Peña, L.A., Smith, J.A.L., Martinez, S.R., Bacarian, T., Tammam, J., Ren, B., Farmer, P.M., Kalef-Ezra, J., Micca, P.L., Nawrocky, M.M., Niederer, J.A., Recksies, F.P., Fuchs, A., Rosen, E.M., 2002. Response of rat intracranial 9L gliosarcoma to microbeam radiation therapy. Neuro-Oncology 4, 26–38.

Laissue, J.A., Geiser, G., Spanne, P.O., Dilmanian, F.A., Gebbers, J.-O., Geiser, M., Wu, X.-Y., Makar, M., Micca, P.L., Nawrocky, M.M., Joel, D.D., Slatkin, D.N., 1998. Neuropathology of ablation of rat gliosarcomas and contiguous brain tissues using a microplanar beam of synchrotron-wiggler-generated x rays. Int. J. Cancer 78, 654–660.

Lee, K.Y., Fung, K.L., Kwok, C.S., 2004. Development and initial evaluation of a spectral microdensitometer for analysing radiochromic films. Phys. Med. Biol. 49, 5171–5183.

McLaughlin, W.L., Chen, Yun-Dong, Soares, C.G., Miller, A., Van Dyk, G., Lewis, D.F., 1991. Sensitometry of the response of a new radiochromic film dosimeter to gamma radiation and electron beams. Nucl. Instrum. Methods A 302, 165–176.

Nariyama, N., 1995. Calculations of energy deposition by low energy electron beams. KEK Proc. 95–9, 1–8.

Nariyama, N., 2005. Responses of GafChromic films for distribution of extremely high doses from synchrotron radiation. Appl. Radiat. Isot. 62, 693–697.

Nariyama, N., Tanaka, S., Nakane, Y., Namito, Y., Hirayama, H., Ban, S., Nakashima, H., 1995. Absorbed dose measurements and calculations in phantoms for 1.5 to 50 keV photons. Health Phys. 68, 253–260.

Nariyama, N., Kishi, N., Ohnishi, S., 2004. Development of a portable free-air ionization chamber as an absolute intensity monitor for high-energy synchrotron radiation up to 150 keV. Nucl. Instrum. Methods A 524, 324–331.

Salvat, F., Fernández-Varea, J. M., Sempau, J., 2006. PENELOPE-2006: a code system for Monte Carlo simulation of electron and photon transport. ISBN 92-64-02301-1.

Siegbahn, E.A., Bräuer-Krisch, E., Stepanek, J., Blattmann, H., Laissue, J.A., Bravin, A., 2005. Dosimetric studies of microbeam radiation therapy (MRT) with Monte Carlo simulations. Nucl. Instrum. Methods A 548, 54–58.

Slatkin, D.N., Spanne, P., Dilmanian, F.A., Sandborg, M., 1992. Microbeam radiation therapy. Med. Phys. 19, 1395–1400.

Slatkin, D.N., Spanne, P., Dilmanian, F.A., Gebbers, J.-O., Laissue, J.A., 1995. Subacute neuropathological effects of microplanar beams of X-rays from a synchrotron wiggler. Proc. Natl. Acad. Sci. USA 92, 8783–8787.

Tanaka, T., Kitamura, H., 2001. SPECTRA: a synchrotron radiation calculation code. J. Sychrotron Radiat. 8, 1221–1228.

Stabilities of ^{67}Ga- and ^{111}In-Labeled Transferrin *In Vitro*

Yosuke Ohtake[1,*], Akiko Maruko[1], Yoshikazu Kuwahara[2], Manabu Fukumoto[2] and Yasuhito Ohkubo[1]

[1]*Department of Radiopharmacy, Tohoku Pharmaceutical University, 4-4-1, Komatsushima, Aoba-ku, Sendai, Miyagi 981-8558, Japan;* [2]*Department of Pathology, Institute of Development, Aging and Cancer, Tohoku University, 4-1, Seiryo-machi, Aoba-ku, Sendai, Miyagi 980-8575, Japan*

Abstract: We attempted to develop a stable radiolabeled transferrin (Tf) useful in experimental studies related to Tf receptor. ^{67}Ga and ^{111}In were used as labeling radioisotopes. The results from gel chromatography, dialysis, and electrophoresis showed that ^{111}In-DTPA-Tf was the most stable among the radiolabeled Tfs examined in the present study. ^{111}In-DTPA-Tf was also the most stable radiolabeled transferrin in the blood.

Keywords: Transferrin, radiolabeling, DTPA, ^{67}Ga, ^{111}In.

INTRODUCTION

We have reported that transferrin (Tf) was not involved in the uptake of ^{67}Ga by the inflammatory tissues, such as granuloma [1, 2] and CCl_4-damaged liver [3, 4], whereas Tf is involved in that by normal liver [5] and regenerating liver after partial hepatectomy [6]. We have also reported that ^{111}In entered into hepatocytes after partial hepatectomy [7] and that Tf was not involved in the uptake of ^{111}In into inflammatory tissues but was involved in uptake into liver and spleen [8]. Transferrin and its receptor (TfR) are not only important to iron metabolism but also play role in various biological events.

Tf receptor (TfR) is a very important target for the study to hemochromatosis [9-12] and cell proliferation [13, 14]. It is beginning to be recognised that TfR 1 is a cellular receptor for New World haemorrhagic fever arenaviruses [15] and it has been established that the macrophage cell surface glyceraldehyde-3-phosphate dehydrogenase is a novel TfR [16]. Moreover, targeted drug delivery via TfR-mediated endocytosis pathway is very interesting in the site-specific delivery of anticancer drugs into proliferating malignant cells that overexpress the TfR [17].

A radiolabeled ligand is necessary for experimental and clinical studies related to TfR.

^{67}Ga was used for the radiolabeling of lectins with a bifunctional chelating agent [18]. ^{111}In was also used for the radiolabeling of galactosyl- and mannosyl- neoglycoalbumin [19] or antibody [20, 21] with a chelating agent.

In the present study we attempted to develop a stable radiolabeled Tf useful for experimental and clinical studies related to TfR.

*Address correspondence to this author at the Department of Radiopharmacy, Tohoku Pharmaceutical University, 4-4-1, Komatsushima, Aoba-ku, Sendai, Miyagi 981-8558, Japan; Tel: +81-22-727-0121; Fax: +81-22-275-2013; E-mail: y-ohtake@tohoku-pharm.ac.jp

MATERIALS AND METHODS

Materials

Gallium-67 citrate (^{67}Ga) and indium-111 chloride (^{111}In) were purchased from Nihon Mediphysics Co.Ltd. (Takarazuka, Japan). Diethylenetriaminepentaacetic acid (DTPA) and transferrin (Tf) in the form of human apotransferrin were purchased from Nacalai Tesque (Tokyo, Japan).

Conjugation of DTPA to Tf

DTPA was conjugated with Tf by the reported method [22] with a slight modification. DTPA (100 mg, 0.25 mmole) and triethylamine (125 mg, 1.25 mmole) were dissolved in 2 ml of H_2O at 40°C and the solution was then cooled to 4°C. 28 µl of isobutylchloroformate (0.25 mmole) was added to the solution. The mixture was stirred for 0.5 h in a cold room at 4°C. The resulting mixed carboxycarbonic anhydride of DTPA was then added to a solution of Tf in 20 ml of 0.1 M $NaHCO_3$ (Tf 13.5 mg / ml). The reaction mixture was kept in a cold room at 4°C for 3 days and subsequently dialyzed against 0.1 M acetate buffer (pH 5.0). The Tf fraction was isolated by Sephadex G-50 column chromatography. Fractions corresponding to DTPA-Tf were monitored by the determination of protein content using Lowry-Folin method. DTPA-Tf fractions obtained were combined and freeze dried.

Radiolabeling of DTPA-Tf and Tf with ^{67}Ga and ^{111}In

Radiolabelings of DTPA-Tf and Tf were carried out using carrier free ^{67}Ga and ^{111}In. Each 2 mg of freeze dried DTPA-Tf and Tf were dissolved in 2 ml of saline and incubated with 0.4 ml of the ^{111}In and ^{67}Ga solution (185 kBq / ml) at room temperature for 45 min.

Gel Chromatography of Radiolabeled Tf

The solutions of DTPA-Tf and Tf incubated with ^{67}Ga or ^{111}In were applied to Sephadex G-50 columns equilibrated and eluted with PBS. The flow rate was 0.44 ml / min and

0929-8665/09 $55.00+.00